



저작자표시-비영리-변경금지 2.0 대한민국

이용자는 아래의 조건을 따르는 경우에 한하여 자유롭게

- 이 저작물을 복제, 배포, 전송, 전시, 공연 및 방송할 수 있습니다.

다음과 같은 조건을 따라야 합니다:



저작자표시. 귀하는 원저작자를 표시하여야 합니다.



비영리. 귀하는 이 저작물을 영리 목적으로 이용할 수 없습니다.



변경금지. 귀하는 이 저작물을 개작, 변형 또는 가공할 수 없습니다.

- 귀하는, 이 저작물의 재이용이나 배포의 경우, 이 저작물에 적용된 이용허락조건을 명확하게 나타내어야 합니다.
- 저작권자로부터 별도의 허가를 받으면 이러한 조건들은 적용되지 않습니다.

저작권법에 따른 이용자의 권리는 위의 내용에 의하여 영향을 받지 않습니다.

이것은 [이용허락규약\(Legal Code\)](#)을 이해하기 쉽게 요약한 것입니다.

[Disclaimer](#)

Thesis for the Degree of Master of Science

A Study on Daytime Sea Fog Retrieval  
Algorithm Improvement Using GOCI  
Data



by

Kyung Hun Lee

Department of Environmental Atmospheric Sciences

The Graduate school

Pukyong National University

August 2018

A Study on Daytime Sea Fog Retrieval  
Algorithm Improvement Using GOCI  
Data

GOCI 자료를 이용한 주간 해무 탐지  
알고리즘 개선에 대한 연구

Advisor: Prof. Byung Hyuk Kwon

by

Kyung Hun Lee

A thesis submitted in partial fulfillment of the requirements  
for the degree of

Master of Science

in Department of Environmental Atmospheric Sciences, the Graduate School,  
Pukyong National University

August 2018

A Study on Daytime Sea Fog Retrieval Algorithm  
Improvement Using GOCI Data

A dissertation  
by  
Kyung Hun Lee

Approved by:

---

(Chairman)

Dong-In Lee

---

(Member)

Hong-Joo Yoon

---

(Member)

Byung Hyuk Kwon

August 24, 2018

# Contents

Contents .....	i
List of Figures .....	iii
List of Tables .....	vi
Abstract .....	vii
I . Introduction .....	1
II . Data and Methods .....	5
1. Data .....	5
1.1. GOCI data .....	5
1.2. MI data .....	12
1.3. AWS data .....	15
2. Methods .....	17
2.1. Sea-fog retrieval method .....	17
2.2. Validation method .....	22
2.2.1 Qualitative validation .....	22
2.2.2 Quantitative validation .....	24
3. Site and Cases .....	26
3.1. Sea fog observation .....	26

III. Results and Discussion .....	34
1. False negative of Land fog .....	37
2. False positive of Sea fog .....	47
IV. Conclusion .....	68
Reference .....	70



## List of Figures

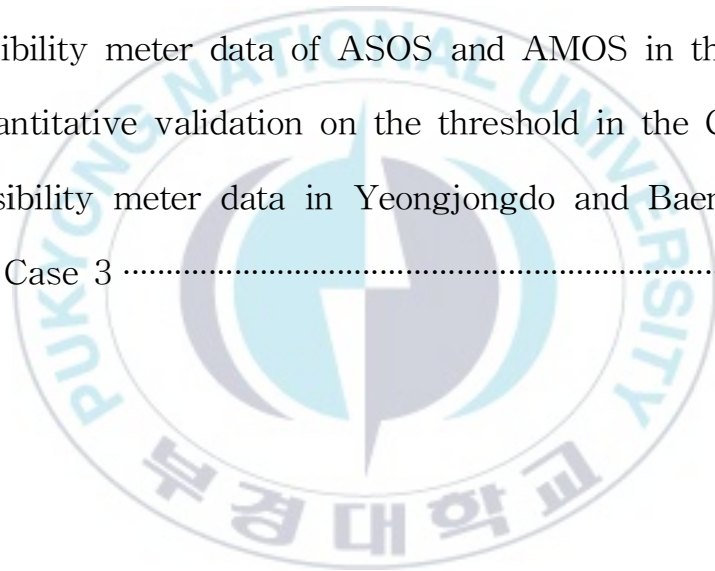
Fig. 1. Area of GOCI data. ....	7
Fig. 2. MI Fog image at 14 LST on May 13 2018. ....	14
Fig. 3. Visibility meter sites (triangle) and visibility map. ....	16
Fig. 4. GOCI color scale image at 14 LST on April 16 2017. ....	18
Fig. 5. GOCI Rrc spectral of each band according to surface different at 14 LST on April 16 2017. ....	18
Fig. 6. GOCI Fog image at 11 LST on May 22 2017. ....	20
Fig. 7. Fog image of MI (left) and visibility map (right). ....	23
Fig. 8. ASOS, AMOS site in the central part of the West Sea. ....	27
Fig. 9. Fog image of MI: 00:45 LST (left), 20:45 LST (right) on May 23 2014. ....	29
Fig. 10. 850 hPa weather chart (KMA) at 09 LST on May 23 2014. .....	30
Fig. 11. Fog formation at Yeongjongdo (KMA) on February 11 2015. .....	32
Fig. 12. 850 hPa weather chart (KMA) at 09 LST on April 04 2017. .....	33
Fig. 13. GOCI color scale image (left), Rrc spectral distribution of Band 6 and Band 7 along red line (right) at 09 LST on May 01 2014. ....	35
Fig. 14. Himawari-8 visible image at 09 LST on April 04 2017. ....	36

Fig. 15. Band 6 and Band 7 Rrc distribution of Baengnyeongdo (left) and Yeongjongdo (right). Black pixels indicate land under a clear sky. The green indicates the island's boundary at 09 KST on April 04 2017. ....	36
Fig. 16. Frequencies of Band 7 Rrc on the west coast (on April 09 2016, on May 06 2016, on June 12 2016). ....	38
Fig. 17. Fog image of MI (left) and visibility map (right) in the Case 1. ....	40
Fig. 18. Visibility map for the Case 2. ....	41
Fig. 19 Case. 1. GOCI fog image before threshold applied(left) and after threshold applied(right). ....	43
Fig. 20. GOCI fog image without threshold (left) and with threshold (right) in the Case 2. ....	44
Fig. 21. Fog image of MI in the Case 3 (Baengnyeongdo). ....	46
Fig. 22. GOCI fog image without threshold (left) and with threshold (right) of Baengnyeongdo in the Case 3. ....	46
Fig. 23. Rrc spectrum profiles for each band over the sea without clouds. ....	48
Fig. 24. Area for greater Band 4 Rrc than the Band 8 Rrc. ....	50
Fig. 25. GOCI fog image by index III at 09 LST on May 23 2014. ..	50
Fig. 26. Visibility map at 09 LST on May 23 2014. ....	51
Fig. 27. MI fog image at 09 LST on May 23 2014. ....	51
Fig. 28. Cluster sampling of cloud pixels. ....	53

Fig. 29. MBR output flowchart. ....	53
Fig. 30. Comparison of the MBR in (a) cloud over sea, (b) sea fog, and (c) lower cloud (stratus). ....	55
Fig. 31. Box-and-whisker plot of three groups (false fog, fog, stratus). ....	58
Fig. 32. Scatter plot of false fog and stratus (upper) and of false fog and fog (lower). The red line shows linear trend. ....	60
Fig. 33. Ascending scatter plot of false fog and stratus (upper) and of False fog and fog (lower). The red line shows linear trend. .....	61
Fig. 34. GOCI fog image after MBR method applied in the Case 1. ·	63
Fig. 35. GOCI fog image before (left) and after (right) MBR method application in the Case 3. ....	65
Fig. 36. Visibility map (left) and MI fog image (right) in the Case 3. .....	66
Fig. 37. GOCI sea fog identification algorithm applying Band 7 threshold and MBR. ....	67

# List of Tables

Table 1. Band characteristics of GOCI .....	9
Table 2. GOCI products .....	10
Table 3. CMDPS data .....	13
Table 4. Contingency table for the four indices of fog detection .....	24
Table 5. Visibility meter data in the Case 1 .....	40
Table 6. Quantitative validation on the threshold in the Case 1 .....	41
Table 7. Visibility meter data of ASOS and AMOS in the Case 2 ..	43
Table 8. Quantitative validation on the threshold in the Case 2 .....	44
Table 9. Visibility meter data in Yeongjongdo and Baengnyeongdo in the Case 3 .....	45



# GOCI 자료를 이용한 주간 해무 탐지 알고리즘 개선 연구

이 경 훈

부 경 대 학 교 대 학 원 환 경 대 기 과 학 과

## 요 약

GOCI(Geostationary Ocean Color Imager)는 8개 밴드의 레일리 보정된 반사율을 이용하여 수평 500m x 500m의 높은 공간해상도로 동아시아 지역을 관측한다. 6개의 가시광선(Band1~6)과 2개의 근적외선 밴드(Band7~8)는 표면(육지, 바다, 구름 등)의 특성에 따라 반사율이 달라지는 특징이 있어, 이를 통해 해무를 탐지할 수 있다. 그러나 반사율을 이용한 방식은 하층운과 해무를 구별하기 어렵다는 단점을 가지고 있다. 최근에 수증기 흡수영역의 반사율 차이를 이용한 방법이 제시되었으나 육무 오염지 및 해무 과탐지 문제가 발견되어 본 연구에서 이를 개선코자 하였다.

관측된 표면의 반사율 특성과 선행 연구의 해무탐지 알고리즘에서 각각의 표면을 구별하는 지수들을 분석한 결과, 육지는 근적외선 밴드가 가시광선 밴드보다 반사율이 크게 나타나고, 바다는 가시광선 밴드의 반사율이 크게 나타났다. 구름에도 이런 특징이 반영되어 육지 위에 있는 구름은 Band7, 바다 위의 구름은 Band6의 반사율이 크게 나타나며, 이로 인해 육무 오염지와 해무 과탐지 문제가 발생한다. 육무 오염지 문제는 해무와 하층운의 액체함수량 차이를 이용한 Band7 반사율 임계값을 적용하여 육지로 유입되는 해무를 하층운으로 탐지하는 문제를 개선하였다.

해상의 구름 중 바다와 같이 Band4가 Band8의 반사율보다 크게 나타나는 구름은 해무로 탐지되어 해상에서 해무 과탐지를 일으킨다. 이러한 구름을 주변 구름픽셀과의 평균 반사율인 MBR(Mean Band Rrc) 비교를 통해 보정해줌으로써 해무 과탐지 문제를 개선하였다. 개선 결과는 천리안위성 COMS(Communication, Ocean, Meteorological Satellite)의 기상 탑재체인 MI(Meteorological Imager) 안개 영상과 시정 분포도 자료를 이용하여 안개 탐지 영역을 비교하였고, 기상청 시정계 지점 자료를 통해 안개탐지확률(POD: Probability of Detection), 안개오탐지율(FAR: False Alarm Ratio), 안개탐지수준(KSS: Hanssen-Kuiper Skill Score), 안개탐지정확성(TS: Threat Score)을 산출하여 개선 정도를 정량적으로 검증하였다.

# I . Introduction

Fog is formed when the water vapor adjacent to the ground condenses around the condensation, nucleus indicated when the visibility is less than 1 km (KMA, 2015). Generally, the diameter of fog particles is 5~40  $\mu\text{m}$ , and particles of 1  $\text{cm}^3$  include 10~30 water droplets. The visibility decreases with increasing amounts of water droplets and also decreases due to scattering effect when the number of particles is smaller (Yang and Oh, 2005). The formation and dispersion of fog is influenced by the surrounding geographical or meteorological conditions, and the density or thickness of fog is affected by the humidity, temperature, wind, type of condensation nucleus, etc. (Kim, 1998). According to the generation mechanism, fog is classified as radiation, upslope, advection, frontal, or steam fog, which have different characteristics such as generation time, location, and duration (Kim et al., 1995). The fog is highly variable in time and space because it is influenced by complex interactions from the microscale to the synoptic scale (Lee and Suh, 2018). The fog has effects on the temperature and moisture conditions and therefore, fog causes changes in vegetation and forests. In addition, the fog under stable and stagnant atmospheric conditions arouses worse air quality (Darko, 2017). It can also cause social and economic problems, such as

traffic accidents and flight cancellations (Cho, 2003).

Until recently, many domestic and international studies have been implemented to predict the formation and dispersion of fog. Studies have mainly been conducted to determine the natural features of fog based on the thermodynamics, chemistry, and microphysical processing analysis (Li et al., 2001; Sheng et al., 2003; Gultepe et al., 2007). In Korea, studies have been implemented to analyze fog, which has seasonal and regional characteristics. These include studies on the frequency and duration of fog in Korea (Mun and Lee, 2013) and on the effect of local wind on inland fog (Shim and Lee, 2017). Furthermore, in order to predict the occurrence of fog, research using numerical models (Kim et al., 2003; KMA, 2015).

"Sea fog" means formed fog from the sea, most of which belongs to the category of advection fog. Sea fog mainly occurs on the west coast in Korea during the summer months of May to July and with decreasing frequency in the order of spring, fall, and winter (Byun et al., 1997). Sea fog causes disturbances to coastal roads, ships, and aircraft operation by decreasing the visibility (Kim et al., 2011). Recently, accidents caused by the sea fog for instance, the Yeongjong Grand Bridge 106-car collision, the stranded ferry at Heuksando, and the cancelled flights at Incheon and Gimpo airports.

A number of studies have been implemented to characterize and detect sea fog. These include analysis on the characteristics of the atmospheric and oceanic factors in the event of sea fog on the Yellow Sea (Woen et al., 2000) and retrieval of sea fog data using

Multi-functional Transport Satellite (MTSAT) and Advanced Microwave Scanning Radiometer (AMSR) (Park and Kim, 2012).

Currently, the Korean Meteorological Administration (KMA) has obtained visibility data by installing 279 visibility meters nationwide as of 2016 to research and observe fog (KMA, 2016). However, it is difficult to install observation equipment at sea and it is limited to detect local fog with meteorological instruments fixed on land. Therefore, remote sensing such as satellites is needed (Heo et al., 2008). In Korea MI on the Communication, Ocean, Meteorological Satellite (COMS) is used to retrieve the fog data. Advanced countries in meteorology like Japan and the U.S.A also use the Himawari-8 satellite and Advanced Very-High-Resolution Radiometer (AVHRR) and Moderate-Resolution Imaging Spectroradiometer (MODIS) sensors to observe the fog. In general, the observation of fog by satellite is the Dual Channel Difference (DCD) method, which uses the difference in the brightness temperature between two channels (Eyre et al., 1984; Ellord, 1995; KMA, 2015), and the Temperature Difference Index (TDI) method, which uses the difference in the temperature between clouds and the sea surface (Jeon, 2016).

Sea fog retrieval method of Geostationary Ocean Color Imager (GOCI) is use Rayleigh Corrected Reflectance (Rrc). According to the characteristics of the surface (land, sea, cloud, etc.), having a characteristic that difference the 8 band's Rrc, through this we can detected sea fog. GOCI has the advantage of real-time observation during the daytime with high spatial resolution on the Korean

peninsula. In addition, detecting sea fog using the reflectance of visible ray is useful in the ocean with low surface reflectance. However, it is too difficult to distinguish between sea fog and the lower cloud because both have similar characteristics. Recently, a method using the difference in the Liquid Water Content (LWC) between the sea fog and stratus has been reported (Yuan et al., 2016). This method is useful to observe sea fog that could not be observed with MI at the moment of the Yeongjong Grand Bridge accident. However, when sea fog flowed onto land, it is improperly categorized as stratus and sea fog. Therefore, this paper seeks to improve these two problems.

Chapter 1 introduces the necessity for sea fog research, prior studies on the topic, and methods using satellites. Chapter 2 introduces the data used in this study and describes the method for problem solving. Chapter 3 presents the study and validation results following the research method. Finally, the conclusion summarizes the aforementioned studies and presents the usefulness of daytime sea fog observation and future research directions.

## II. Data and Methods

### 1. Data

When detecting or predicting fog, the physical and dynamic characteristics of fog must be considered using a prediction model and a statistical model, which are numerical models (Byun et al., 1997). Satellites observe fog that was already generated; hence, this study did not classify the types of fog according to meteorological elements. Moreover, low visibility from rainfall or snowfall was not considered and visibility under 1 km was assumed to be attributable to fog. Although the fog observed on islands or shores cannot all be treated as sea fog (Heo and Ha, 2004), this study regarded them all as sea fog since there are no distinct characteristics that can physically differentiate them.

#### 1.1. GOCI data

GOCI is the world's first geostationary satellite. It was launched in June 2010 and observes the East Asian region (2500 km × 2500 km

around the Korean Peninsula) for 8 h (00~07 UTC) using a temporal resolution of 1 h intervals at a high spatial resolution of 500 m × 500 m (Fig. 1). GOCI consists of 6 visible domains from Band 1 to Band 6 and bands near-infrared domains from Band 7 to Band 8 (Table 1). The GOCI's observation principle uses sunlight reflections through visible ray remote sensing (Yoon, 2018). Images are detected using a 2-dimensional detector through taring method, and images are taken 8 times from 00 UTC to 07 UTC for 30 min daily from Band 1 to Band 8 followed by 30 min of rest. The images are sent to the Korea Ocean Satellite Center (KOSC) and are integrated as digital data.



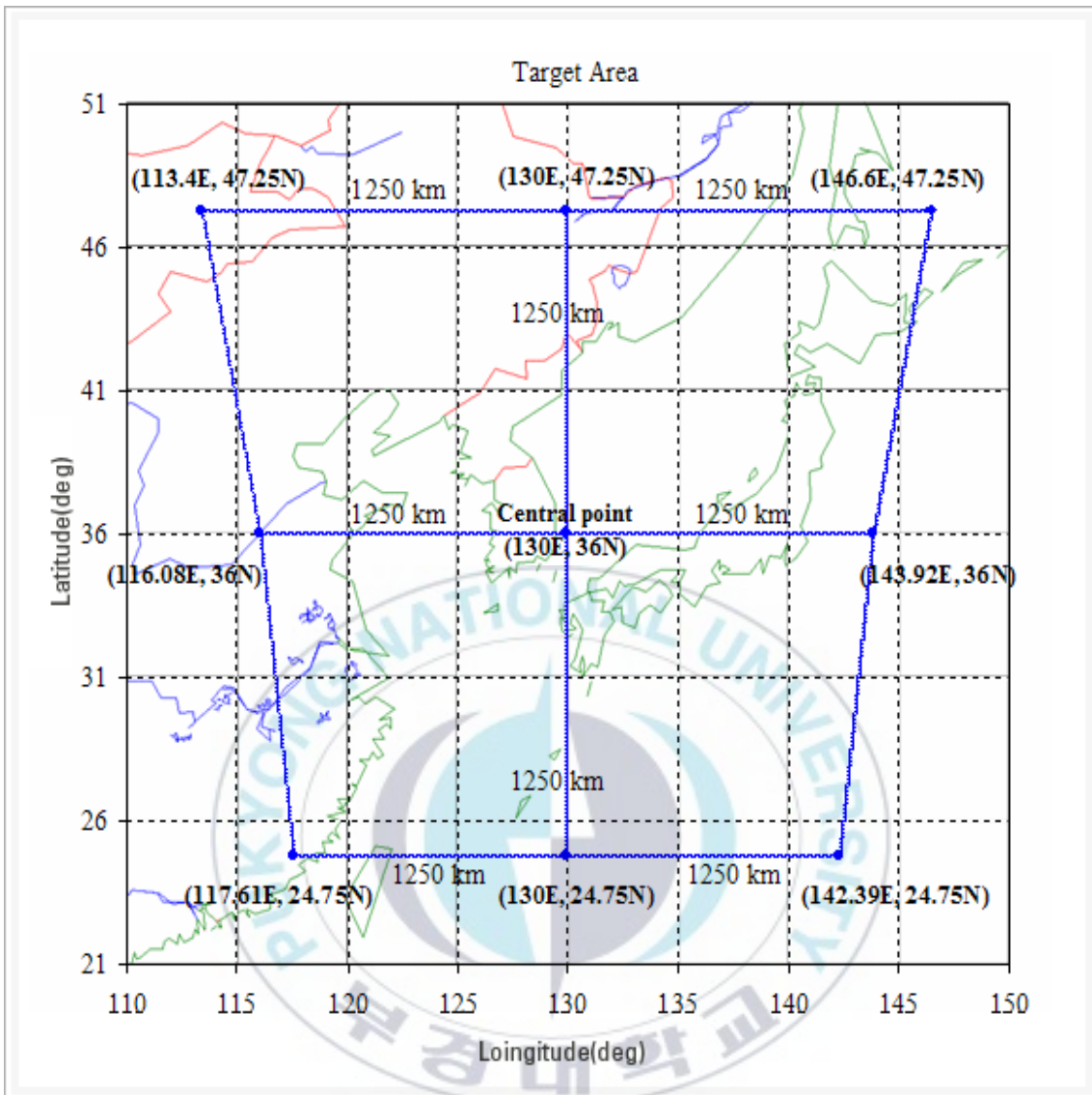


Fig. 1. Area of GOCI data  
(KOSC: Korea Ocean Satellite Center).

Table 2 shows the 37 different types of data that are calculated through the GOCI data-processing system (GDPS), including 13 types of Lv2-A (including flags), 5 types of Lv2-B, 1 type of Lv2-C, 10 types of Lv2-P, 5 types of Lv3, and 3 types of Lv3-P. This study used Rayleigh Corrected Reflectance (Rrc) data from Lv2-C to conduct research on sea fog and fog detection.



**Table 1. Band characteristics of GOCI (KOSC)**

Band	Central Wave length	bandwidth	SNR	Primary Application
1	412 (Visible)	20	1000	Yellow substance turbidity
2	443 (Visible)	20	1190	Chlorophyll absorption maximum
3	490 (Visible)	20	1170	Chlorophyll and other pigments
4	555 (Visible)	20	1070	Turbidity, suspended sediment
5	660 (Visible)	20	1010	Baseline of fluorescence signal, chlorophyll, suspended sediment
6	680 (Visible)	10	870	Atmospheric correction and fluorescence signal
7	745 (NIR)	20	860	Atmospheric correction and baseline fluorescence
8	865 (NIR)	40	750	Aerosol optical thickness, vegetation, water vapor reference over the ocean

Table 2. GOCI products (KOSC)

Level	Abbreviation	Description	Unit
L2A	LW (8)	Radiation intensity by band	W/m <sup>2</sup> /um/sr
	NLW (8)	Normalized radiation intensity by band	W/m <sup>2</sup> /um/sr
	KD490	Extent of solar energy being diffused as it gets deep down into seawater	m <sup>-1</sup>
	CDOM	Amount of organic substance dissolved in seawater	m <sup>-1</sup>
	CHL	Chlorophyll concentration included within plant plankton in seawater	mg/m <sup>3</sup>
	TSS	Amount of floating inorganic matter in seawater	g/m <sup>3</sup>
	RI	Degree of red tide generation	-
	VIS	Extent of horizontal clearness of water	m
	LAND_EVI	Index that represents the vitality of vegetation	-
	LAND_NDVI	Normalized Difference vegetation index	-
	DUST_FMF	Value that represents the aerosol property and that is used to detect yellow sand in the sea	-
DUST_AOT	Yellow dust - aerosol optical thickness	-	
L2B	A (4)	Absorption coefficient in four bands of 400 ~500nm	m <sup>-1</sup>
	A_PHYTO (4)	Chlorophyll absorption coefficient in four bands of 400~500nm	-
	A_SEDI (4)	Suspended matters absorption coefficient in four bands of 400~500nm	-
	A_CDOM (4)	Colored dissolved organic matter absorption coefficient in four bands of 400~500nm	-
	BB (4)	Inverse diffusion coefficient in four bands of 400~500nm	m <sup>-1</sup>
L2C	Rrc (8)	Remove rayleigh scattering in aerosol reflectance	-

Table 2. Continued

L2P	RRS (8)	Remote sensing reflectance	sr <sup>-1</sup>
	BF (8)	Correction of change in value caused by sunlight and sensor	-
	Longitude	Longitude value for each pixel	deg
	Latitude	Latitude value for each pixel	deg
	Landmask	Cloud (above land (3), above sea (1)), land (2), sea (0) masking information	-
	PHV	Satellite azimuth for each pixel	deg
	THV	Satellite zenith angle for each pixel	deg
	SOLA	Solar azimuth for each pixel	deg
	SOLZ	Solar zenith angle for each pixel	deg
	COSSZ	Solar zenith angle for each pixel to the cosine direction	-
L3	FGI	Information on fishery based on food quantity and surface sea temperature (MI, NOAA etc.)	-
	WQL	Coastal water quality grade index	-
	PP	Calculation of daily primary productivity	mg C / m <sup>2</sup> /d
	WCV	Created as a separate file (*.TXT)	-
	DP	Duplicate selected information out of L2A based on eight pieces of observational data	-
L3P	SST	Sea surface temperature	deg
	PAR	Photosynthesis active radiation	-
	DL	Length of a day	-

## 1.2. MI data

Chollian is Korea's first geostationary satellite; it is a COMS that performs oceanographic observation, weather observation, and communication duties. The meteorological imager is composed of a radiometer that scans on two axes. A sensor module takes observations with one visibility channel and four infrared channels. An electricity module transmits data and receives commands.

The visible channel takes visibility images at a spatial resolution of 1 km using a peak wavelength of 0.67  $\mu\text{m}$ . The infrared channel uses the luminance temperature (K) and takes short-wave infrared images, vapor images, infrared-1 images, and infrared-2 images at a spatial resolution of 4 km. The peak wavelength of short-wave infrared images is 3.75  $\mu\text{m}$ , 6.75  $\mu\text{m}$  for vapor images, 10.8  $\mu\text{m}$  for infrared-1 images, and 12.0  $\mu\text{m}$  for infrared-2 images (NMSC, 2013).

The COMS Meteorological Data-Processing System (CMDPS) has 16 types of products that are all shown in Table 3. This study used the fog analysis image data provided by the Meteorological Satellite Center to compare the GOCI sea fog detection results and the sea fog domain (Fig. 2).

**Table 3. CMDPS data (NMSC: National Meteorological Satellite Center)**

Computation Sources	Contents
Cloud detection	Presence of clouds information
Clear sky radiance	Estimation of radiation level in cloud-free region
Atmospheric motion vector	Trace movement path of water vapor
Sea surface temperature	Sea surface temperature
Land surface temperature	Land surface temperatures of regions in East Asia
Sea Ice/Snow detection	Estimate sea ice & snow covered regions
Insolation	Solar energy reaching the ground
Upper tropospheric humidity	Vapor amount in the upper troposphere
Total precipitable water	Total vapor amount in troposphere
Cloud analysis	Estimation of shapes & amount of clouds & characteristics of cloud particles
Cloud top temperatures & heights	Estimate the temperatures & heights at the cloud tops
Fog	Fog detection by separating low cloud and fog
Rainfall intensity	Rainfall intensity depending on the types of clouds
Outgoing long-wave radiation	Estimation of earth's long-wave radiation at the top of the atmosphere
Aerosol index	Observation of Asian dust in the atmosphere
Aerosol optical depth	Estimation of atmospheric turbidity due to aerosol

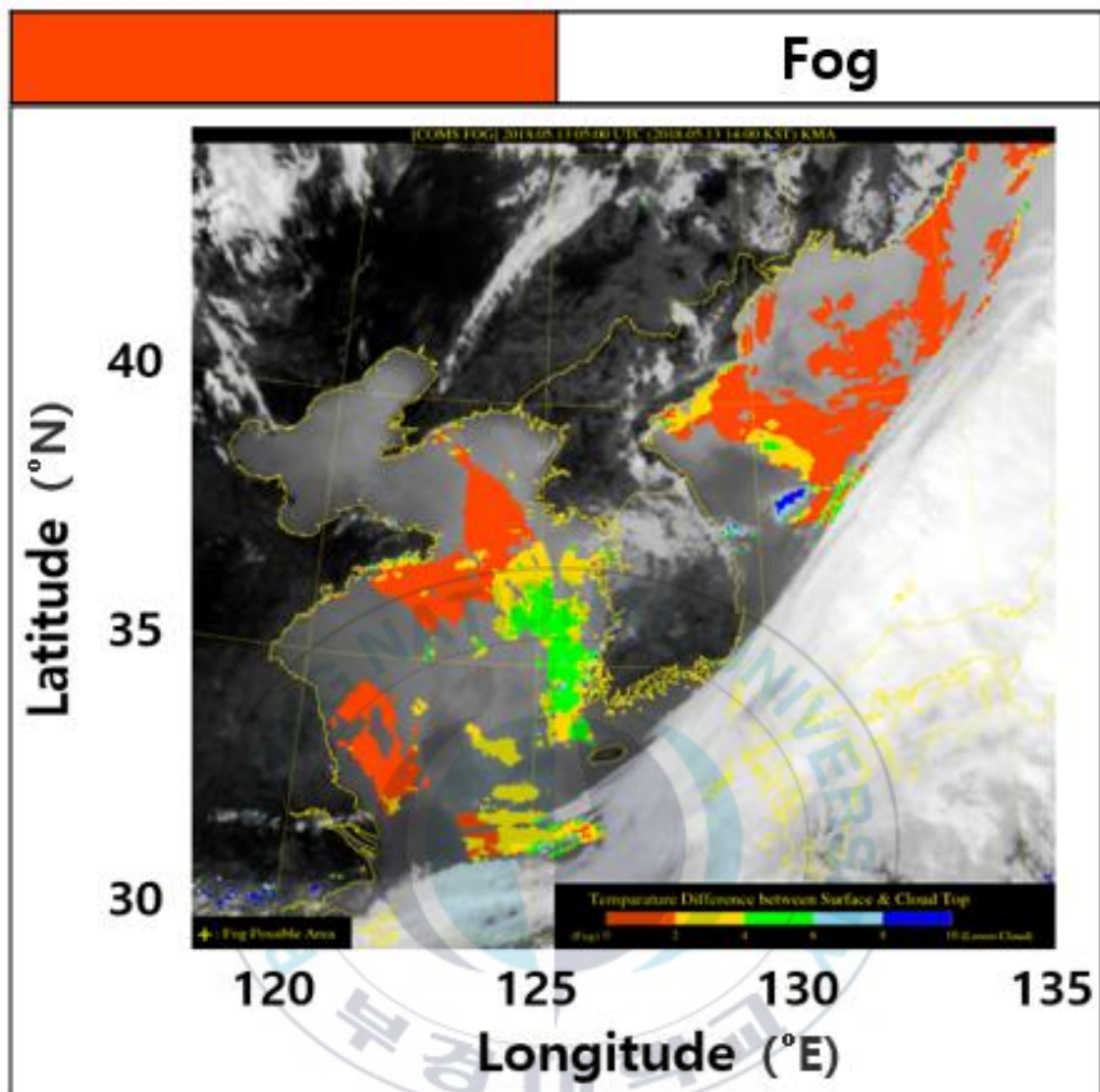


Fig. 2. MI Fog image at 14 LST on May 13 2018.

### 1.3. AWS data

The Automatic Weather System (AWS) observes the atmosphere near the ground in real time. As of 2018, the AWS is installed in over 490 sites nationwide to automatically observe the local temperature, wind, precipitation, etc. Visibility meters are installed in select sites so that they are distributed evenly nationwide from the Automated Synoptic Observing System (ASOS), Aerodrome Meteorological Observation System (AMOS), and AWS sites. The KMA provides visibility data that was observed through the visibility meters installed nationwide, and offers data on visibility, humidity, shilling altitude, and actual weather conditions at 10 min intervals and the nationwide visibility distribution through the fog system of the Automatic Local Weather Information System (ALWAIS) and the comprehensive fog- and smoke-detection system. This study used the visibility meter site data and visibility distribution that are provided by the KMA (Fig. 3). The fog domains at the waterfront and inland areas were compared using the visibility distribution, and visibility data was used to determine whether fog occurred and to calculate verification indices.

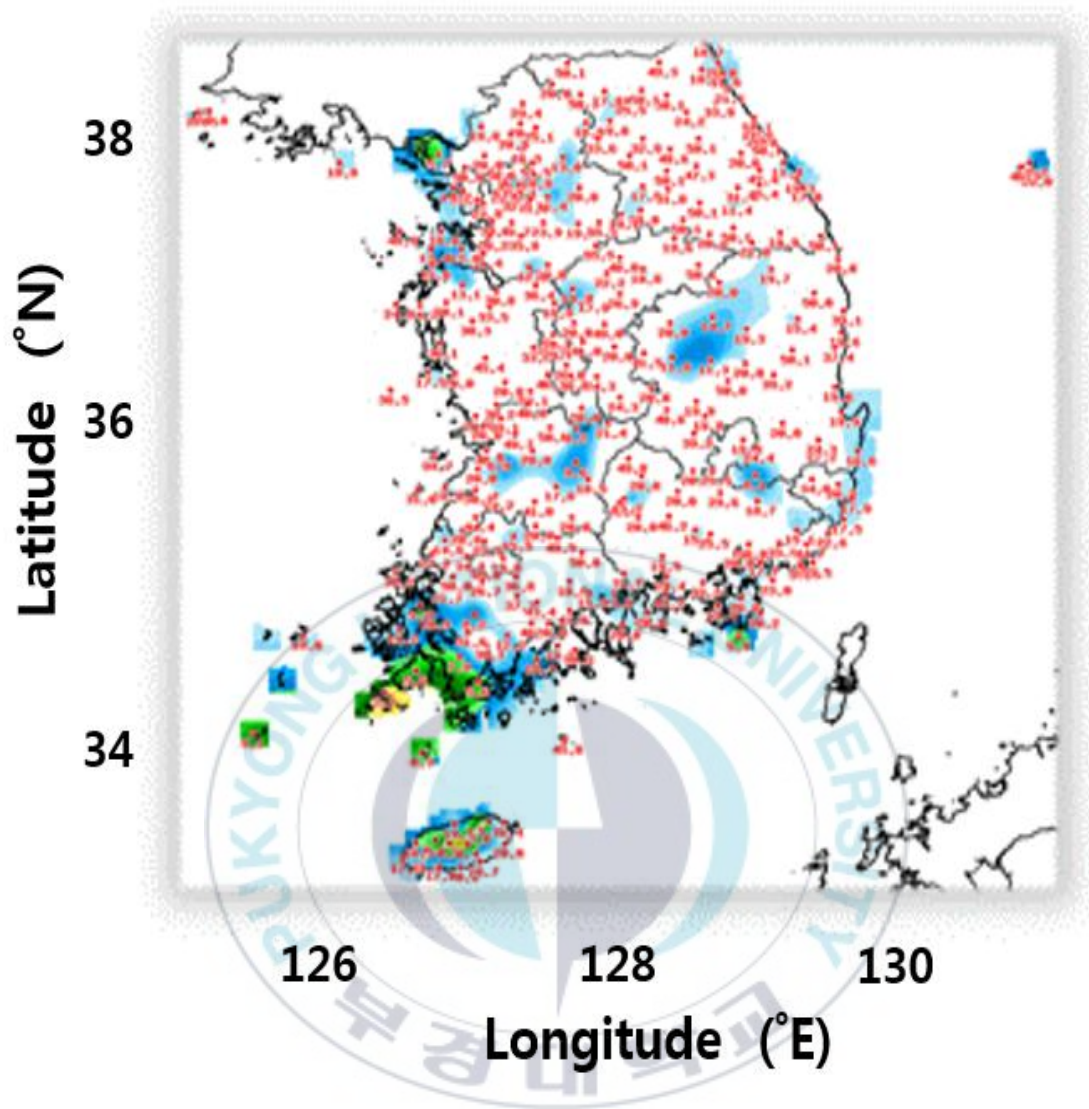


Fig. 3. Visibility meter sites (triangle) and visibility map (KMA).

## 2. Methods

### 2.1. Sea fog retrieval method

In general, the sea fog is detected by the reflectivity of electromagnetic waves transmitted from satellites. The differences of reflectivity in visible rays are classified according to the land, ocean, and clouds. In Fig. 4, upon analyzing the Rrc for each band along the red line on the same latitude, shows surface characteristics. Figure 5 show the Rrc of each band along the red line in Fig. 4. On land, the Rrc shows an ascending trend from Band 1 to Band 8, and in the near-infrared domain band the Rrc is greater than in the visible domain. On the other hand, for the ocean, Rrc is the lowest for Band 8 and Band 7, which are near-infrared domain bands, and the largest at the visible bands of Bands 1~6. For clouds, although there were no distinct characteristics between the visible domain and the near-infrared domain both on land and the ocean, the Rrc at the middle and high-level clouds was high overall.

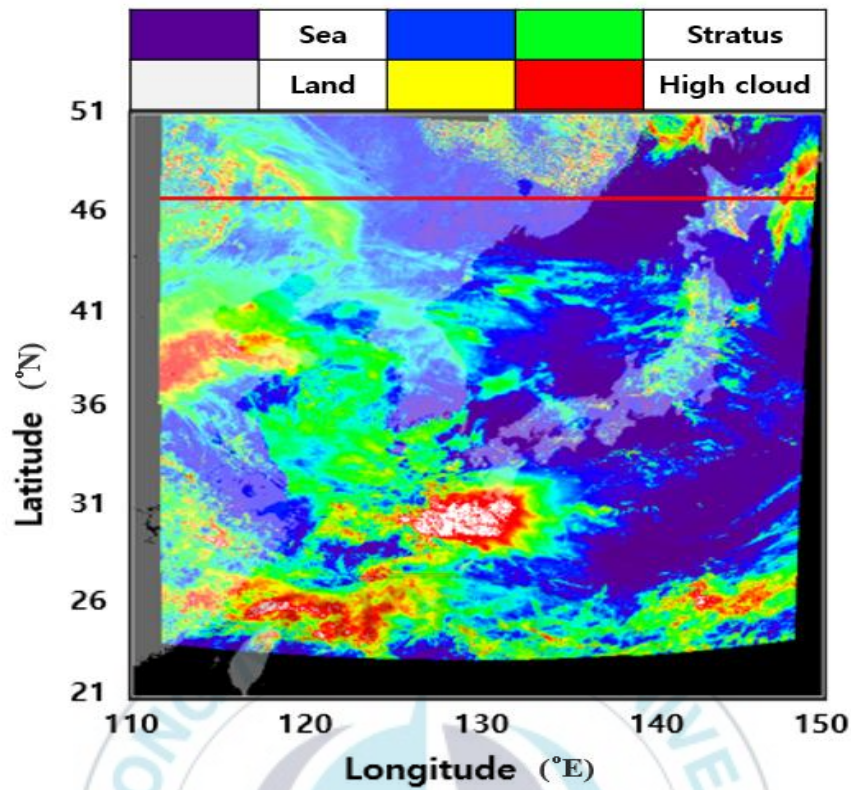


Fig. 4. GOCI color scale image at 14 LST on April 16 2017.

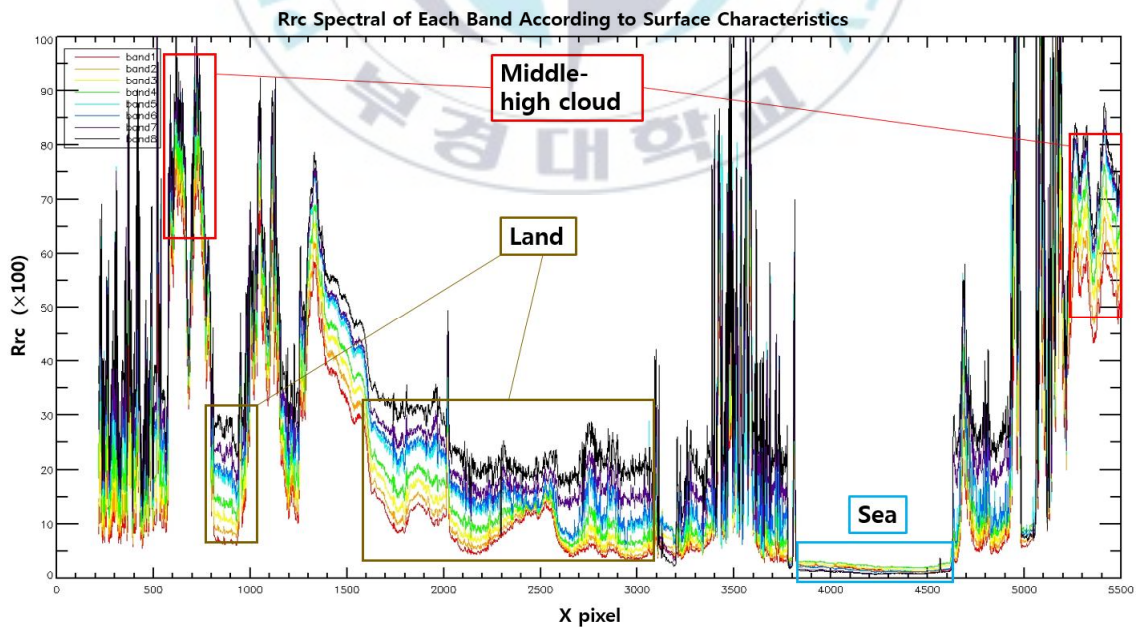


Fig. 5. GOCI Rrc spectral of each band according to surface different at 14 LST on April 16 2017.

With these surface characteristics, we can calculate an index that can differentiate land, ocean, and middle and high-level clouds. First, the index I differentiating the land from the ocean can be calculated by the Rrc of Band 4, which is higher at the ocean, and the Rrc of Band 8, which is lower. The index II that can differentiate middle and high-level clouds can be calculated by high reflectance in clouds.

After determining the land, ocean, and clouds, the fog and lower clouds must be differentiated in order to detect fog. However, because their physical characteristics are similar, it is difficult to differentiate them using sensors equipped on satellites (Bendix et al., 2005). Various methods have been proposed to resolve this issue, including a method that uses the surface data of the MODIS cloud image (Heo et al., 2008) and a method that detects the land fog based on the optical and textural characteristics of fog using MI data (Suh et al., 2017). A recent GOCI-based method was proposed that can differentiate sea fog and lower clouds by the Band Slope Index (Index III): differences in the reflectance of Band 6 and Band 7. However, this method showed a tendency of detecting lower clouds and sea clouds in the Korean Peninsula as sea fog (Fig. 6). The present study improved the land fog misdetection and the sea fog overdetection. Lv2-C Rrc data from KOSC was used and for the periods that lacked data, the Lv1 data was post-processed using GDPS to generate Rrc data. The Rrc data was calculated through Rayleigh scattering correction from GOCI Lv1-B data with a corrected atmosphere.

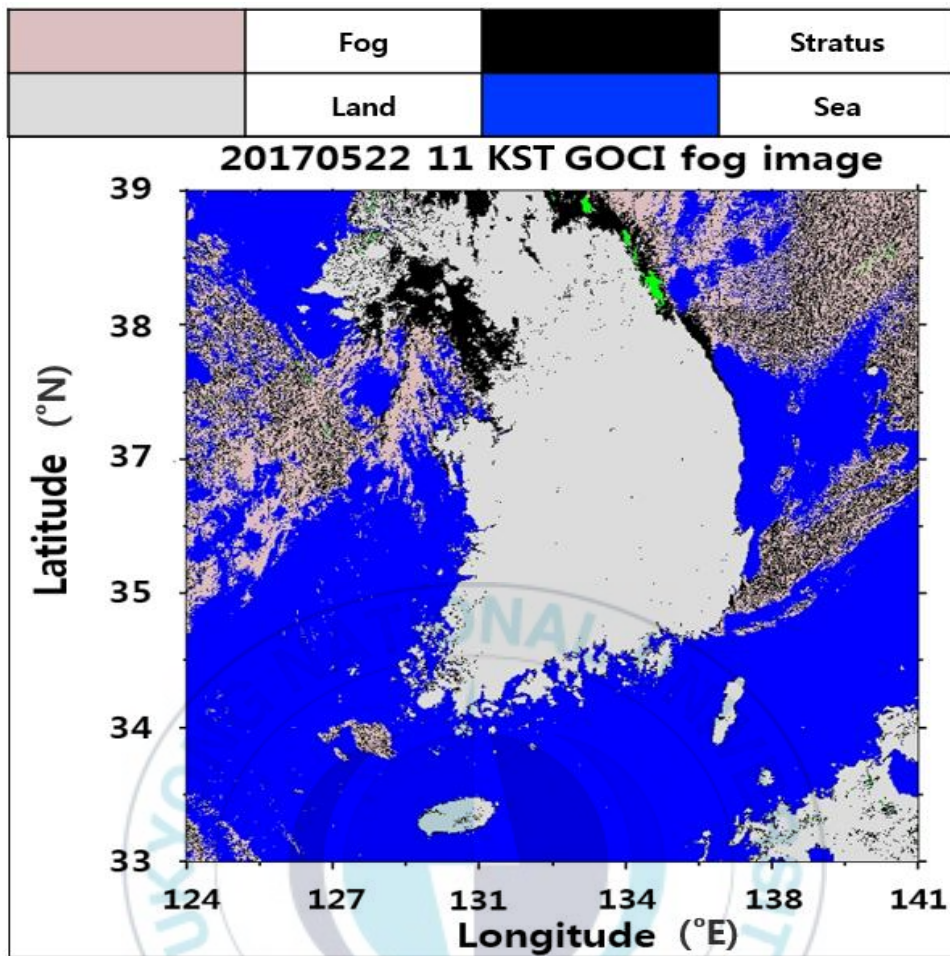


Fig. 6. GOCI Fog image at 11 LST on May 22 2017.

The Index I, which differentiates land and ocean, is calculated through the equation (1). If the value is 0.2 or above, this corresponds to the land, and if the value is -0.2 or below, this corresponds to the ocean. Any values between these values are regarded as clouds. Here, the Rrc of Band 8 and Band 4 refers to the Rayleigh scattering corrected reflectivity of Band 8 and Band 4, which is 865 nm and 555 nm, respectively, for the peak wavelength.

$$index\ I = \frac{Band8\ Rrc - Band4\ Rrc}{Band8\ Rrc + Band4\ Rrc} \quad (1)$$

Index II, which differentiates middle clouds and high-level clouds, is calculated through the equation (2). If the value is 0.6 or above, this corresponds to middle or high-level clouds, and values below that are lower clouds. Here,  $\sum Rrc$  shows the sum of Rrcs from Band 1 to Band 8

$$index\ II = \frac{\sum Rrc}{8} \quad (2)$$

The BSI (Index III) that differentiates sea fog and lower clouds, is calculated through the equation (3). Here,  $\Delta nm$  is the difference in the peak wavelength between Band 7 and Band 6. If the BSI is positive, this corresponds to lower clouds, and a negative value corresponds to sea fog.

$$BSI = \frac{Band7 Rrc - Band6 Rrc}{\Delta nm \times 10e^4} \quad (3)$$

## 2.2. Validation method

### 2.2.1. Qualitative validation

To validate of the sea fog detected by satellites, accurate in-situ data are needed. However, because a visibility meter cannot be installed in the ocean, an indirect method was used by comparing the numerical model with other remote detection equipment. This study used MI fog images (Fig. 7, upper) to verify the accuracy of the sea fog detection domain. The fog domain at the shore and inland was mapped by the visibility distribution (Fig. 7, lower) observed with the visibility meter.

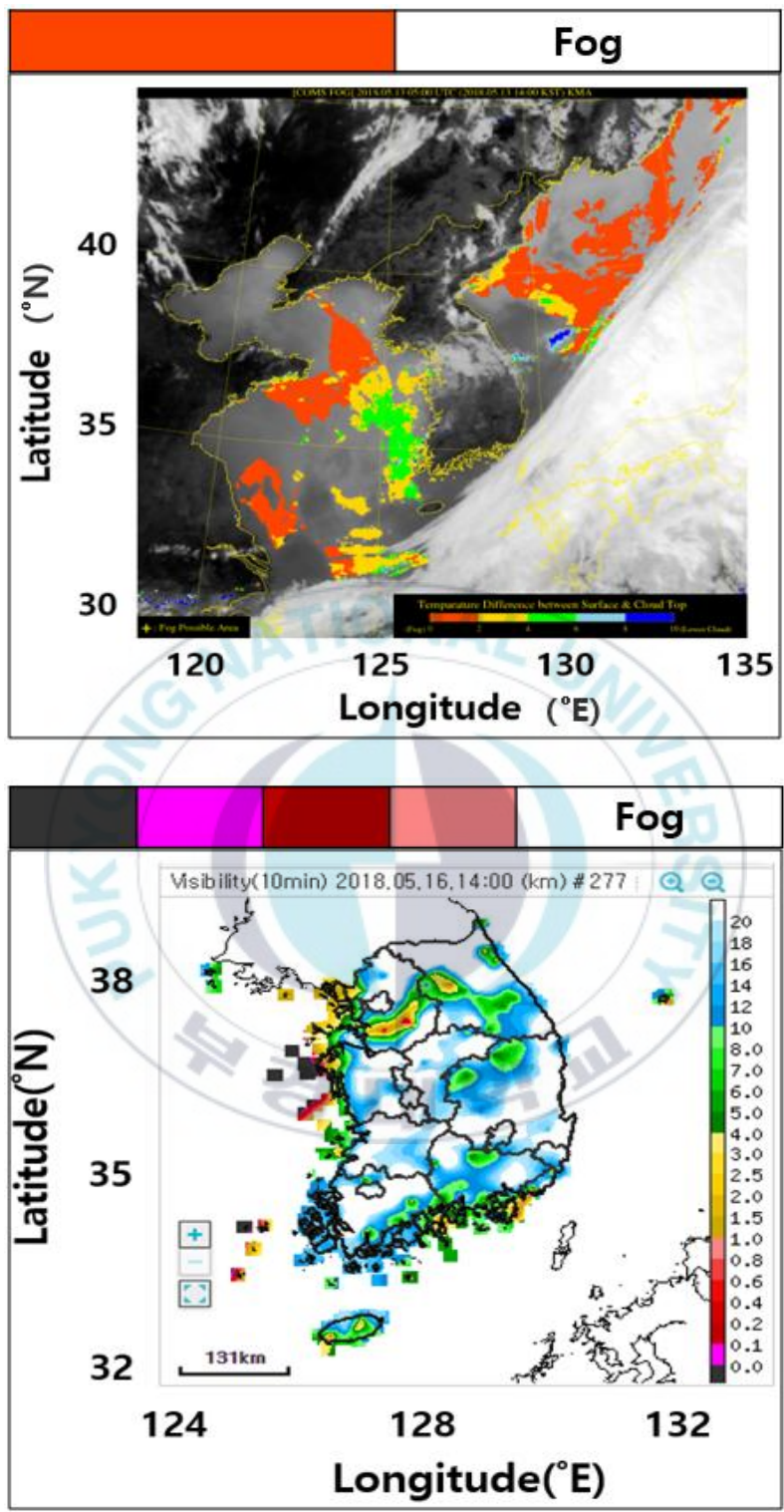
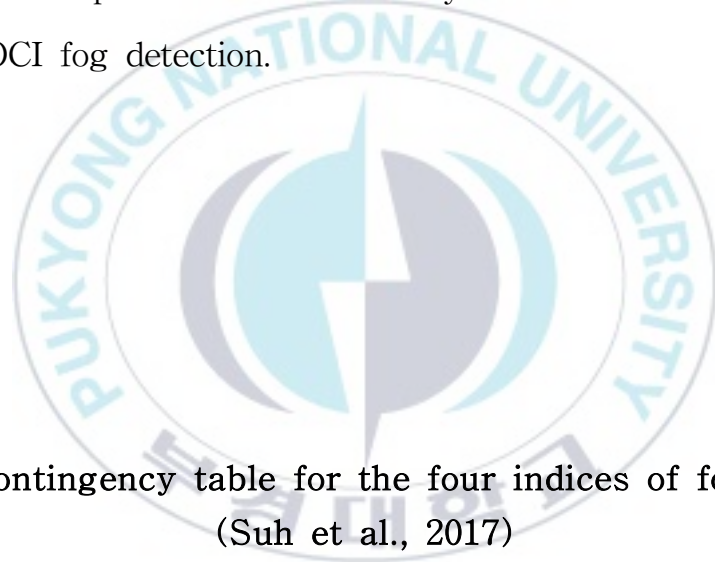


Fig. 7. Fog image of MI (upper) and visibility map (lower).

### 2.2.2. Quantitative validation

The visibility meters installed inland can determine whether fog flowed in or occurred locally. The indices that are typically used to quantitatively evaluate the fog detection level include the Probability Of Detection (POD) and the False Alarm Ratio (FAR) (Suh et al., 2017). These are calculated by comparing the detection results from satellites based on visibility meter observation. We estimated quantitatively the accuracy of fog detection on the nearest GOCI spatial coordinate pixels to the visibility meter. Table 4 shows four indices of GOCI fog detection.



**Table 4. Contingency table for the four indices of fog detection (Suh et al., 2017)**

Contingency table		Visibility detector	
		True	False
GOCI	True	(H) Hit	(F) False alarm
	False	(M) Miss	(C) Correct negative

In the table, "Hit" means fog actually occurred and was detected by the satellite. A "False alarm" is a misdetection, meaning no fog has actually occurred, but fog was detected by the satellite. "Miss" indicates a misdetection, where fog has actually occurred, but the satellite was unable to detect it. "Correct negative" means no fog has occurred, and no fog was detected.

POD shows the fog detection ratio, FAR shows the fog misdetection ratio, KSS (Hanssen-Kuiper Skill Score) is the fog detection level. The closer the value is to -1, the detection level is low, and if the value is closer to 1, the detection level is high. TS (Threat Score) is the fog detection accuracy. The closer the value is to 0, the lower the accuracy, and if it is closer to 1, the accuracy is high.

$$\text{POD} = H / (H+M) \quad (4)$$

$$\text{FAR} = F / (H+F) \quad (5)$$

$$\text{KSS} = \text{POD} - \text{FAR} \quad (6)$$

$$\text{TS} = H / (H+F+M) \quad (7)$$

## 3. Site and Cases

### 3.1. Sea fog observation

The majority of sea fog that flows into Korea occurs in the western sea during the summer from May to July. The central part of the western sea is an area with frequent sea fog because cold air from the north meets the warm current of the south. Moreover, because there are many islands and the Incheon Port, Incheon Airport, and Gimpo Airport are situated there (Fig. 8), disruption from sea fog is a common occurrence due to the thriving activity of airplanes and ships.

We selected sea fog cases on the central area of the western sea. First, data from ASOS, AMOS, and visibility meters was used to analyze cases with a visibility of less than 1 km from 2014–2017 (at 09 LST on May 01 2014, at 09 LST on April 09 2016, at 09 LST on May 06 2016, at 09 LST on June 12 2016, at 09 LST on April 16 2017, at 11 LST on May 22 2017).

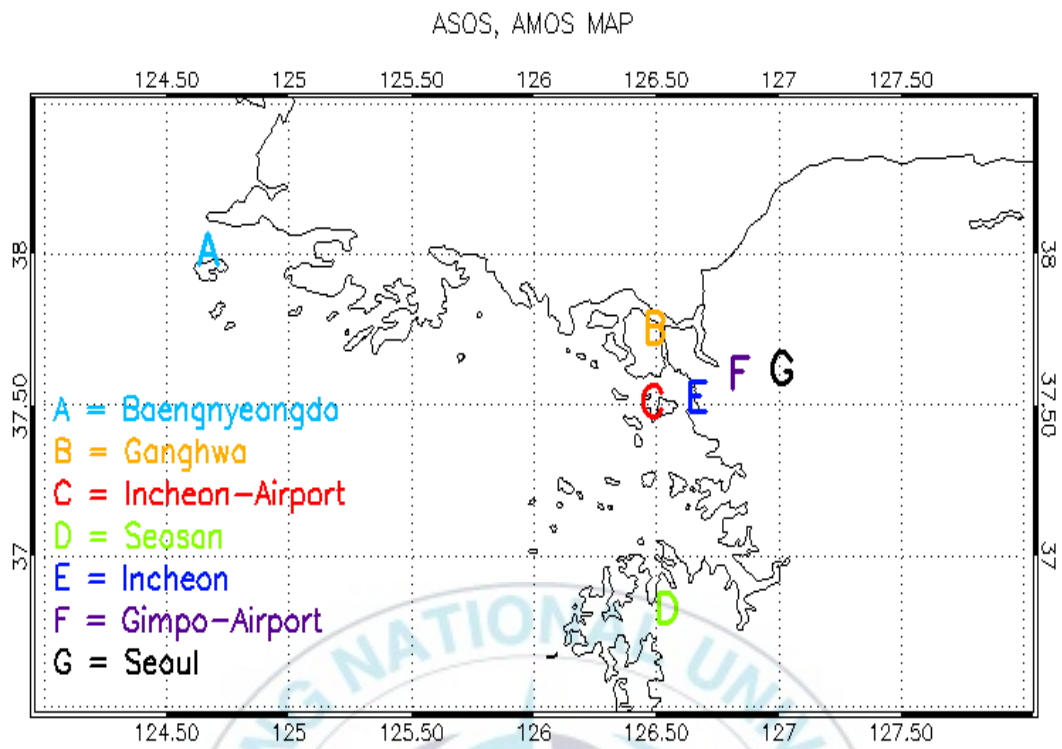


Fig. 8. ASOS, AMOS site in the central part of the West Sea.

In the first case, thick sea fog occurred throughout the entire western sea on May 23, 2014. Thick fog was predicted starting from the day prior, and the KMA issued a fog warning alert. The MI image shows that sea fog persists for almost 20 h (Fig. 9). As high atmospheric pressure with a warm nucleus settled in the Korean Peninsula, the atmosphere became congested, and the continuous inflow from the weak northwestern and western winds caused the formation of a fog, which failed to disperse and became stagnant in the western sea (Fig. 10).



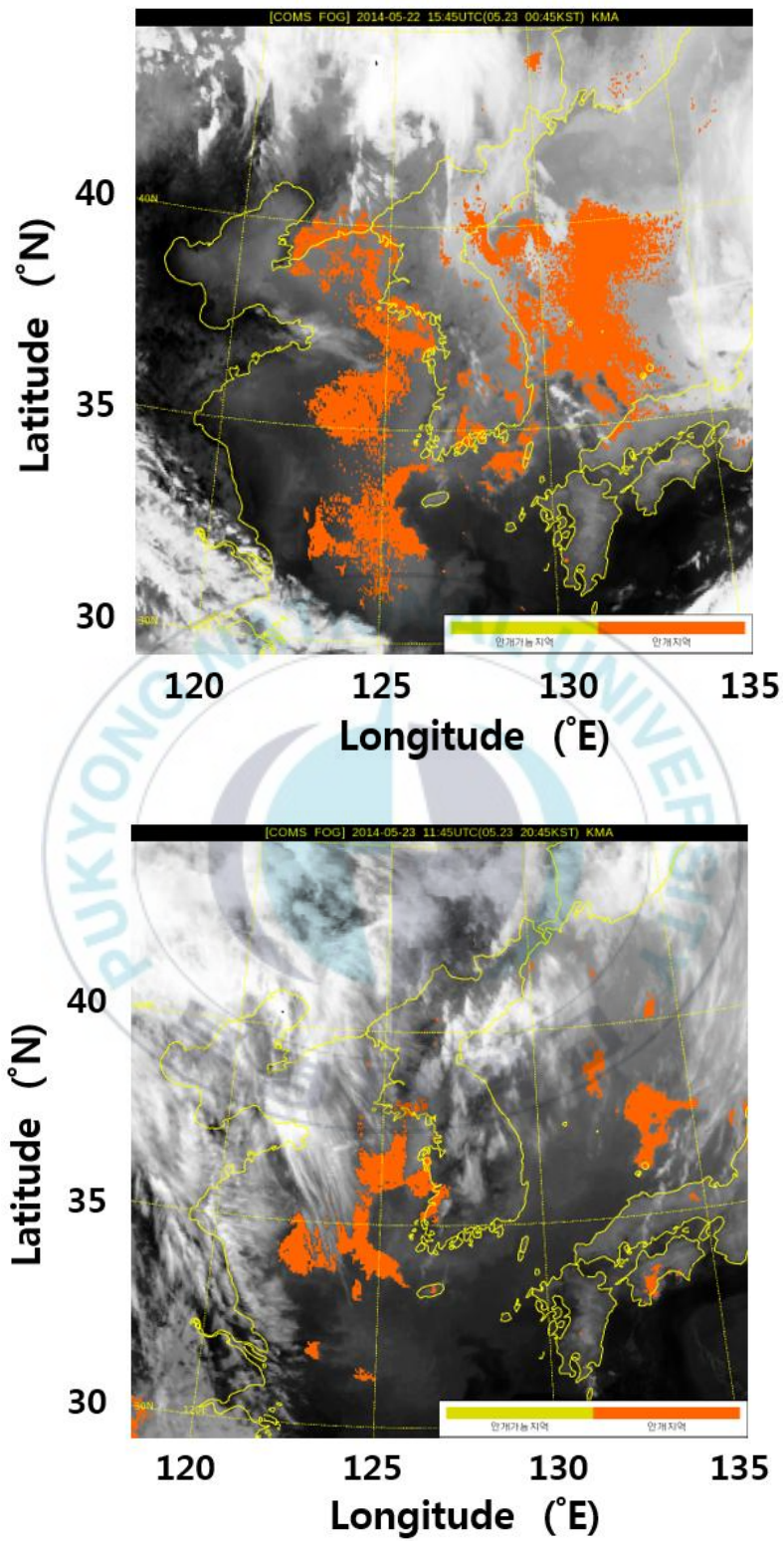


Fig. 9. Fog image of MI: 00:45 LST (upper), 20:45 LST (lower) on May 23 2014.

00UTC 23 MAY 2014 (09KST 23 MAY 2014)

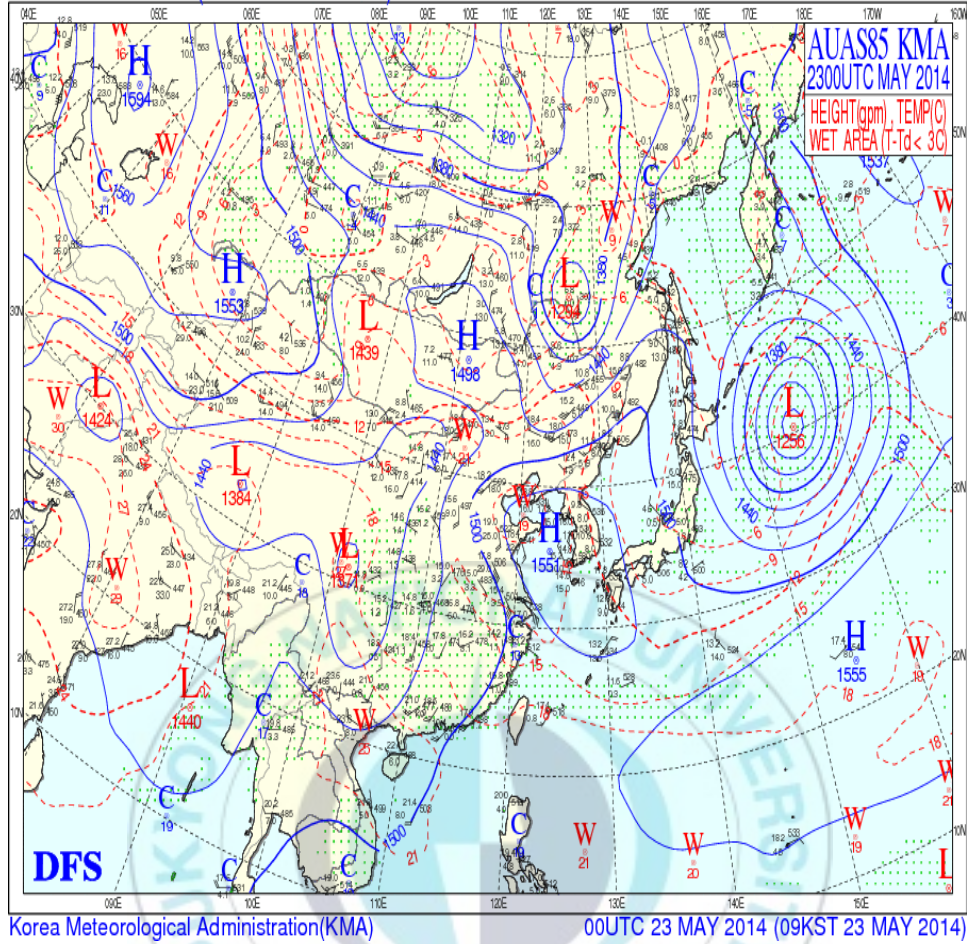
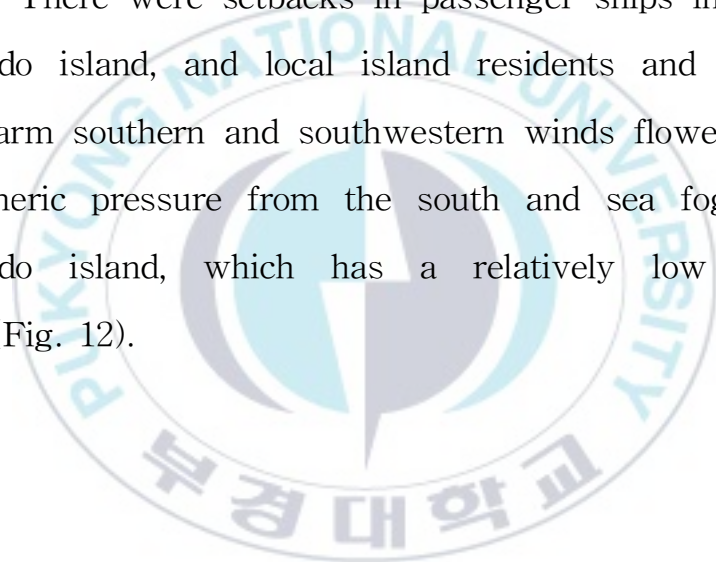


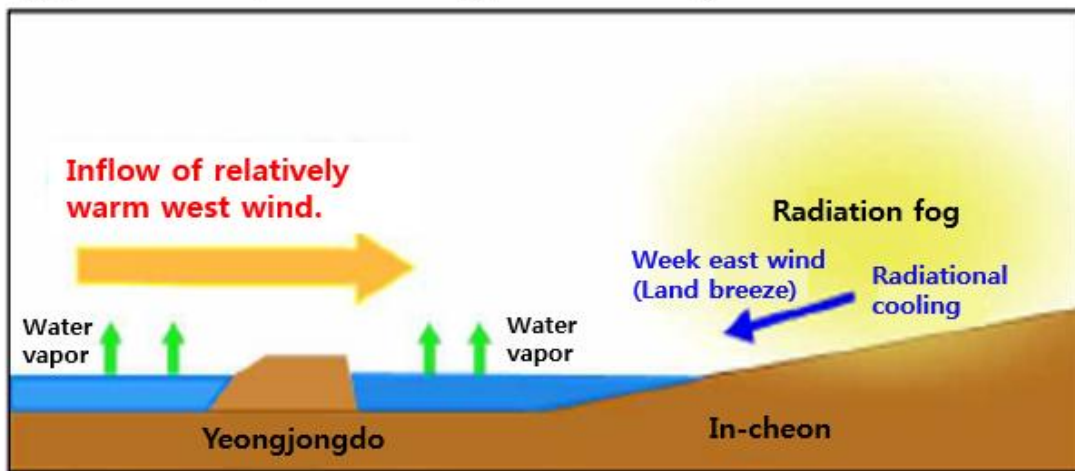
Fig. 10. 850 hPa weather chart (KMA) at 09 LST on May 23 2014.

In the second case, 100 collision accidents occurred at the Youngjong Grand bridge due to sea fog on February 11, 2015. These accidents led to the awareness of sea fog. This sea fog was generated as warm western winds and caused a lake effect in the coastal regions of Yeongjongdo island and Incheon, and the fog grew stronger and persisted due to the constant vapor supply and weak winds (Fig. 11).

In the third case, sea fog occurred at Baengnyeongdo island on May 4, 2017. There were setbacks in passenger ships into and out of Baengnyeongdo island, and local island residents and tourists were fogbound. Warm southern and southwestern winds flowed in from the high atmospheric pressure from the south and sea fog occurred at Baengnyeongdo island, which has a relatively low sea surface temperature (Fig. 12).



**(a) 11th day dawn fog form diagram**



**(b) 11th morning fog form diagram**

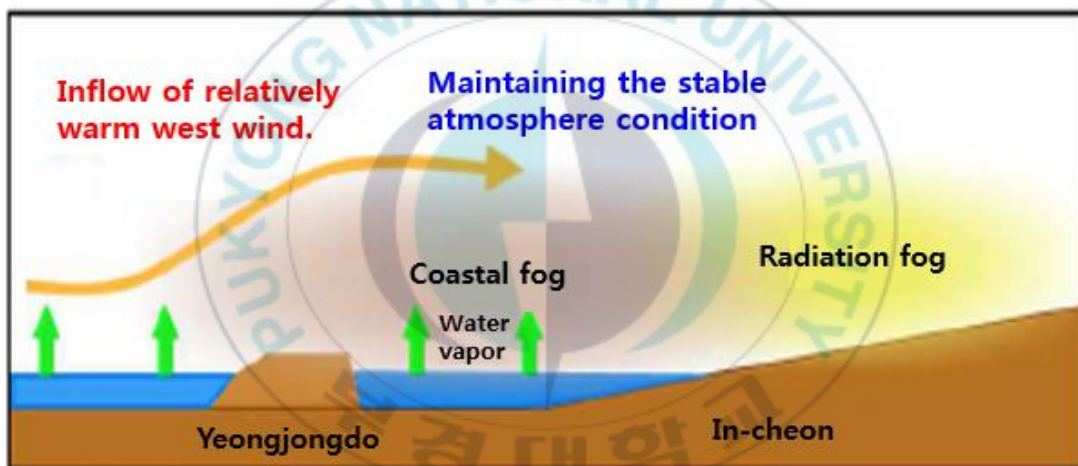


Fig. 11. Fog formation at Yeongjongdo (KMA) on February 11 2015.

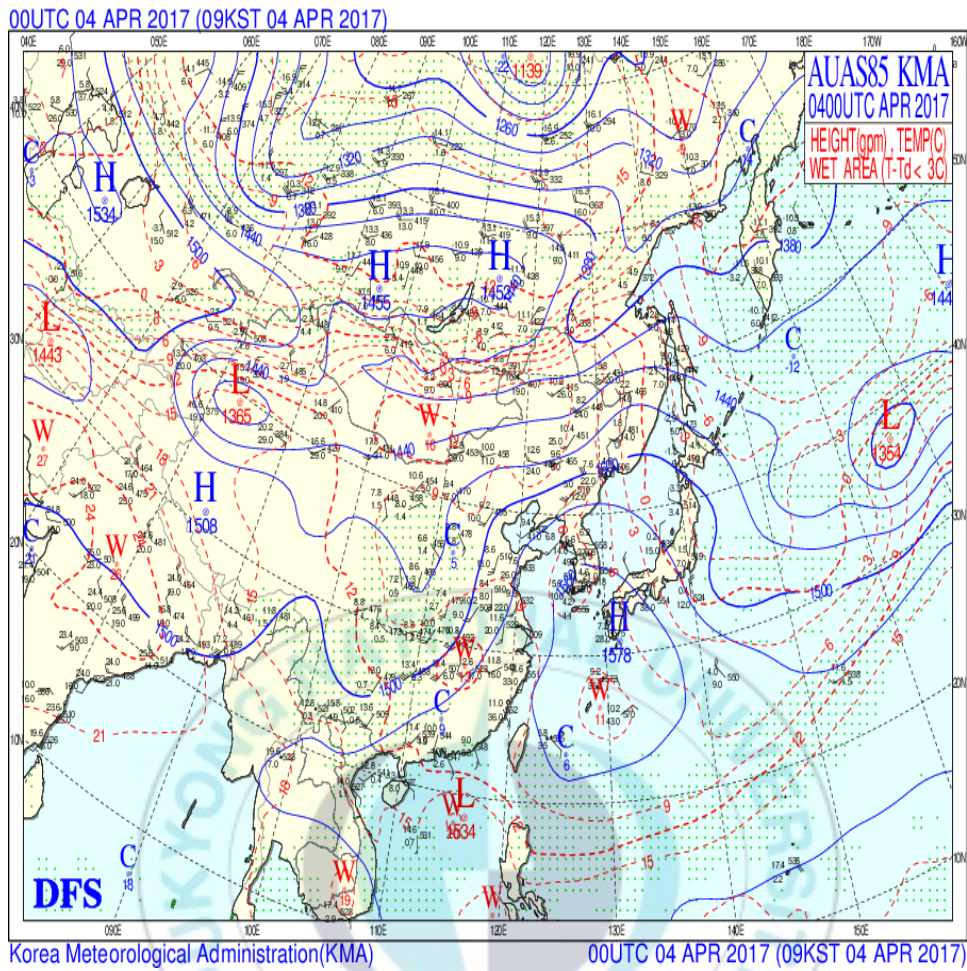


Fig. 12. 850 hPa weather chart (KMA) at 09 LST on April 04 2017.

### III. Results and Discussion

The Rrc of Band 6 and Band 7 were used for index III calculations. As shown in Fig. 13, the Rrc of Band 6 and Band 7 along the red line on the same latitude and longitude, the Rrc of Band 7 is greater than the Rrc of Band 6 on land, and vice versa on sea.

Figure 14 shows clouds over Baengnyeongdo island and Yeongjongdo island, and Figure 15 shows clouds around Baengnyeongdo island and Yeongjongdo island in a line according to the Rrc values. The clouds cover Baengnyeongdo island and Yeongjongdo island with white pixels, but the sea is covered red pixels. This implies that the Rrc of Band 7 is higher for land clouds, like those on land, whereas the Rrc of Band 6 is greater over the sea. In other words, the clouds reflect the characteristics of the land and the ocean that lie below them. Therefore, if sea fog and lower clouds are differentiated only by index III, the majority of land clouds will be distinguished as lower clouds, and the majority of sea clouds will be distinguished as sea fog.

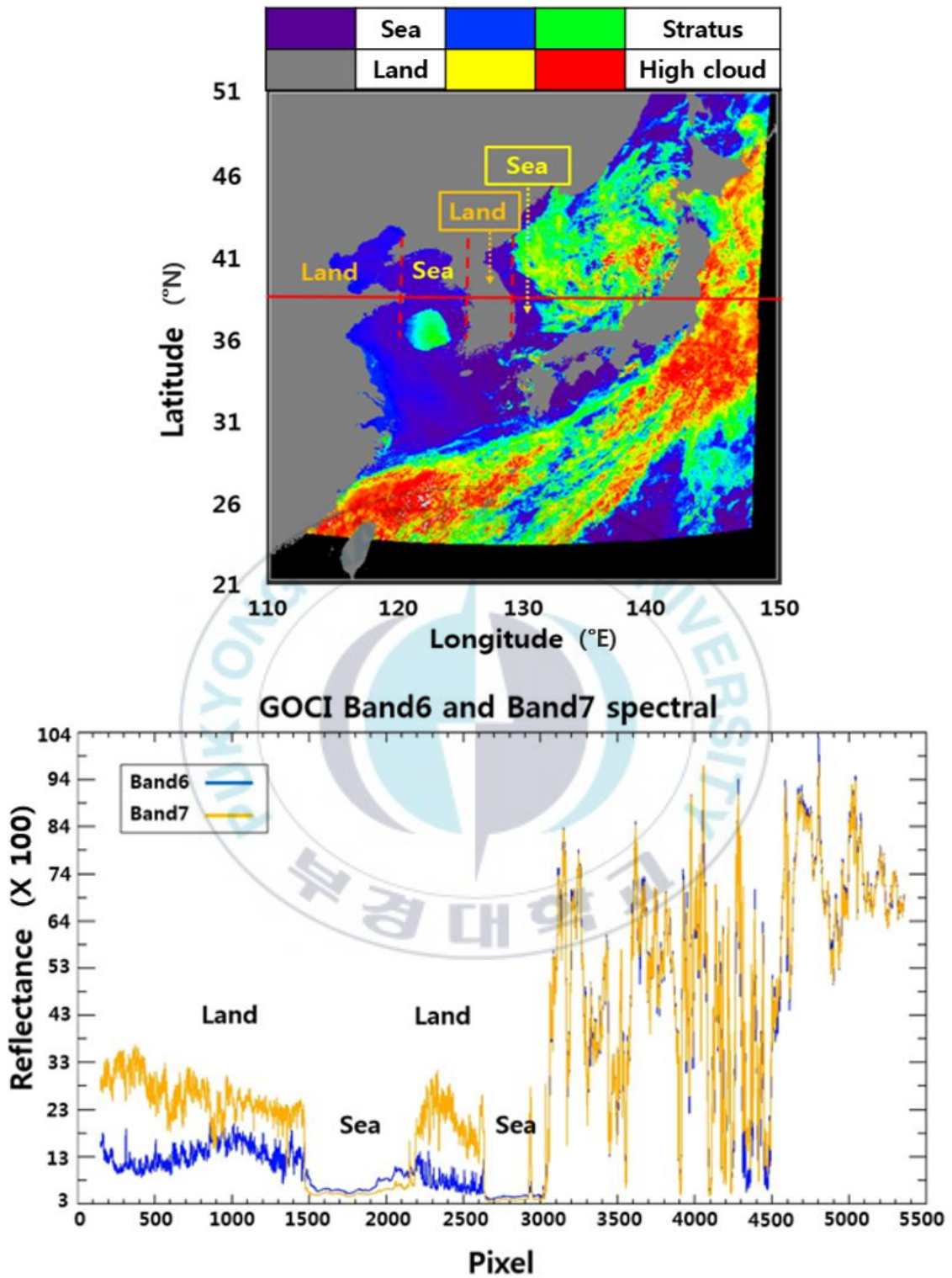


Fig. 13. GOCI color scale image (upper), Rrc spectral distribution of Band 6 and Band 7 along red line (lower) at 09 LST on May 01 2014.

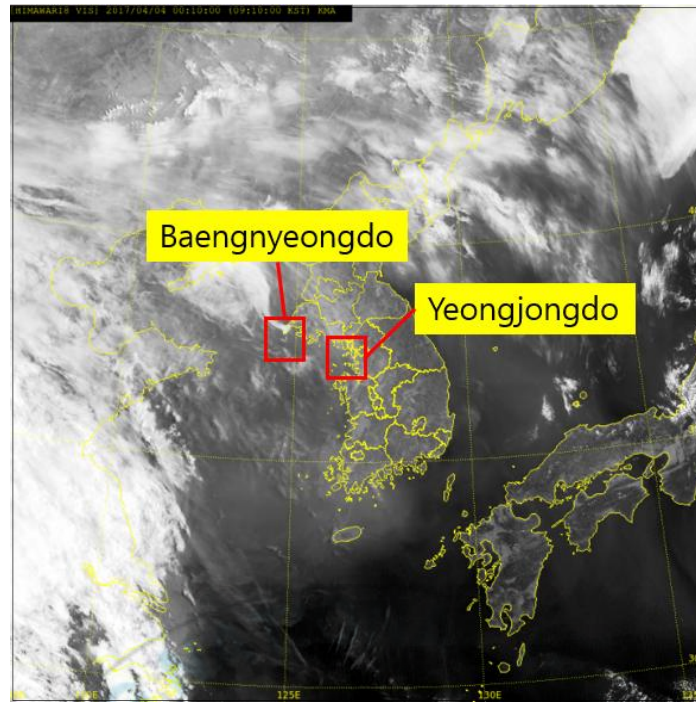


Fig. 14. Himawari-8 visible image at 09 LST on April 04 2017.

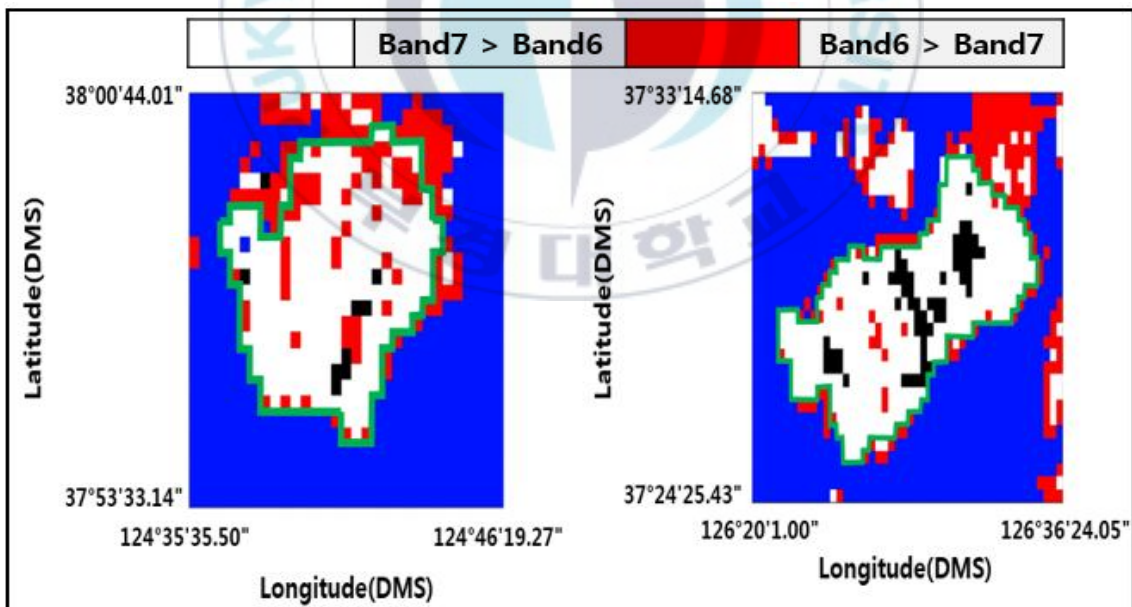
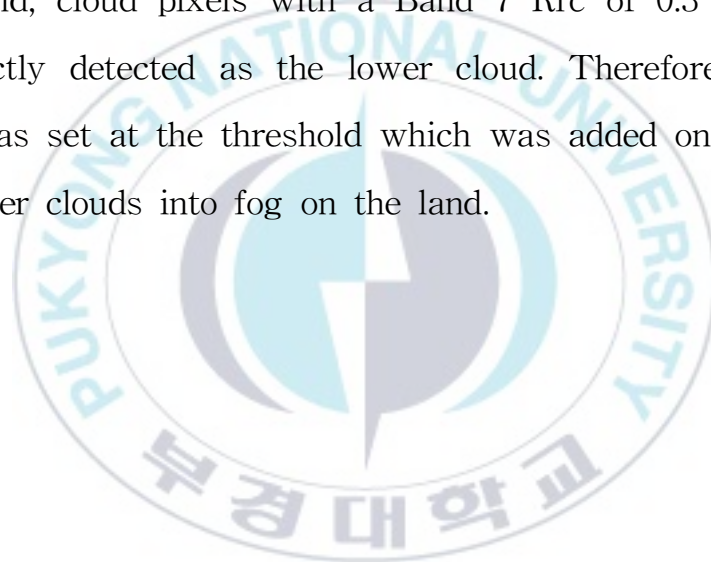


Fig. 15. Band 6 and Band 7 Rrc distribution of Baengnyeongdo (left) and Yeongjongdo (right). Black pixels indicate land under a clear sky at 09 LST on April 04 2017. The green indicates the island's boundary.

## 1. False negative of Land fog

LWC is higher for lower clouds. because their reflectance at the vapor absorption band is less than that of fog (LI, 2001; Sheng et al., 2003). The vapor absorption rate is greater for Band 7 than for Band 6 (Yuan et al., 2016). Most lower cloud pixels (99.6 %) show 0.3 or less of Band 7 Rrc (Fig. 16). Among the pixels considered as lower clouds on land, cloud pixels with a Band 7 Rrc of 0.3 or more have been incorrectly detected as the lower cloud. Therefore, the Band 7 Rrc of 0.3 was set at the threshold which was added on the algorithm to divide lower clouds into fog on the land.



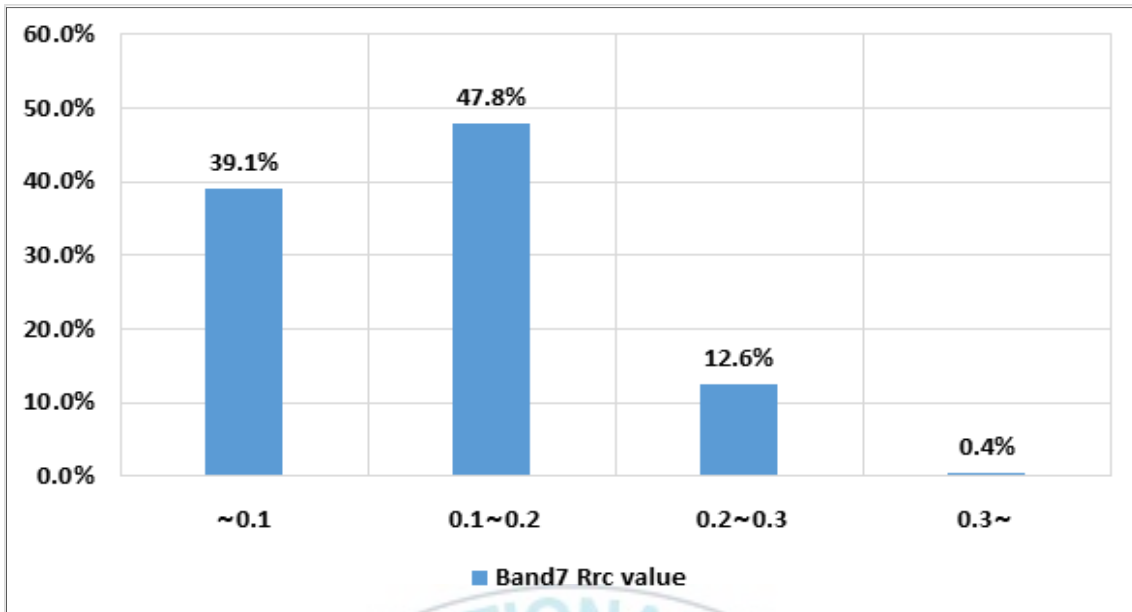
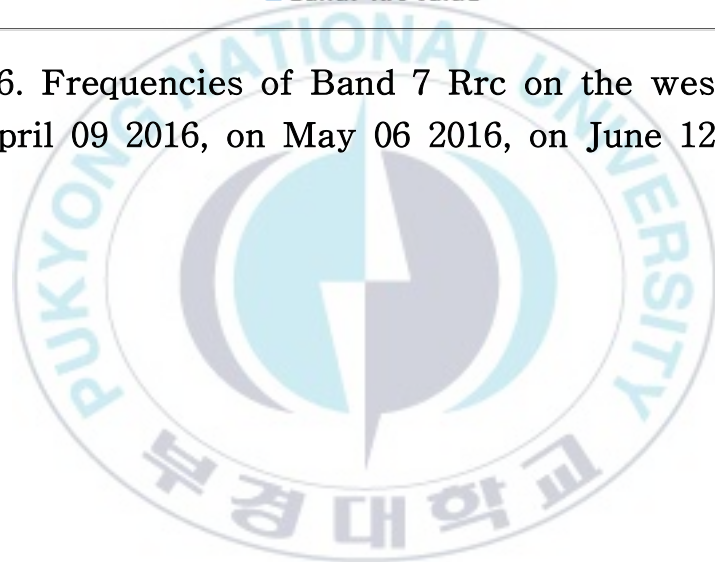


Fig. 16. Frequencies of Band 7 Rrc on the west coast (on April 09 2016, on May 06 2016, on June 12 2016).



The threshold method was applied to the three cases. For the first case, the sea fog was detected in the entire western sea and southern sea based on the MI fog image, and fog was detected throughout Jeollanamdo and Gyeongsangdo near latitudes  $34^{\circ}\text{N}\sim 35^{\circ}\text{N}$  and longitudes  $126^{\circ}\text{E}\sim 128^{\circ}\text{E}$  (Fig. 17, left). In the visibility distribution, fog was observed along the western coast (Fig. 17, right).

The GOCI sea fog detection results after applying the threshold are consistent with the MI fog image. However, before the threshold was applied, fog was not detected at sites where fog was detected on MI fog image (Table 5) (Fig. 18, left). On the other hand, after the threshold was applied, the fog domain near latitudes  $34^{\circ}\text{N}\sim 35^{\circ}\text{N}$  and longitudes  $126^{\circ}\text{E}\sim 128^{\circ}\text{E}$  are consistent with the MI fog image (Fig. 18, right).

The quantitative verification with three indices shows 0.25–0.75 of POD, 0.75–0.67 of FAR, -0.5–0.08 of KSS and 0.14–0.3 of TS (Table 6). While there was no major change in the misdetection rate, the detection rate, detection level, and detection accuracy had improved. This implies that the threshold is useful in detecting the sea fog that flows into the western sea.

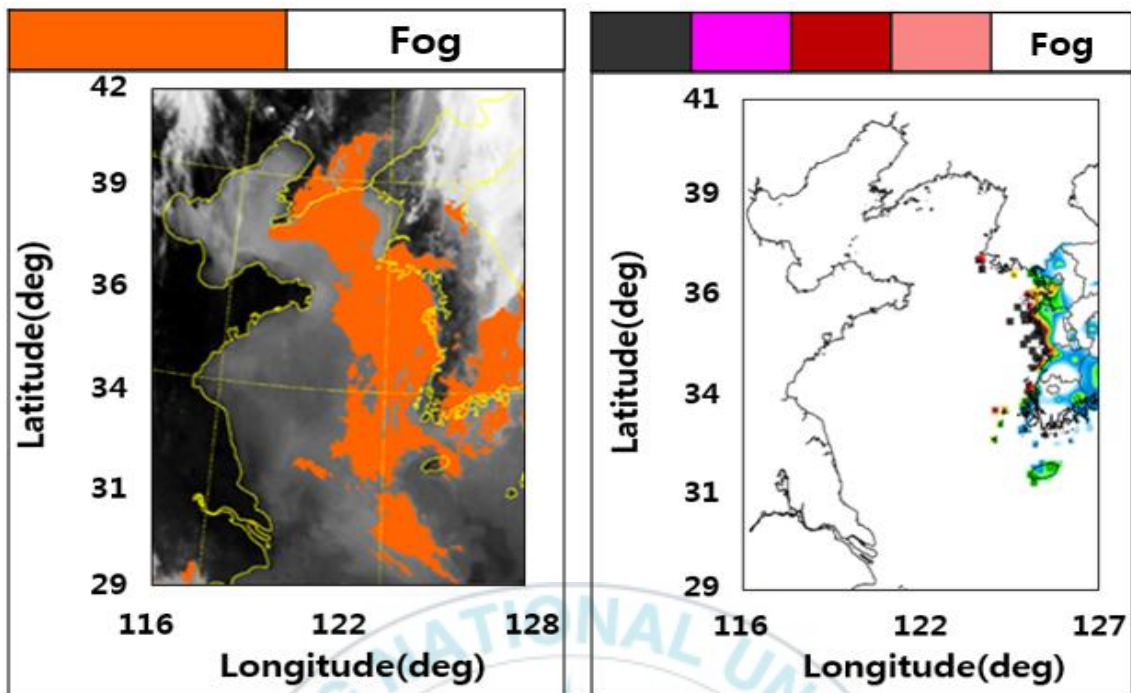


Fig. 17. Fog image of MI (left) and visibility map (right) in the Case 1.

Table 5. Visibility meter data in the Case 1

Site	Date	Visibility
Baengnyeongdo	2014/05/23 09:10 KST	100 m
Heuksando	2014/05/23 09:10 KST	300 m
Boryeong	2014/05/23 09:10 KST	800 m
Yongyeon	2014/05/23 09:10 KST	300 m
Haeju	2014/05/23 09:10 KST	250 m
Gwacheon	2014/05/23 09:10 KST	130 m
Yeomsan	2014/05/23 09:10 KST	960 m

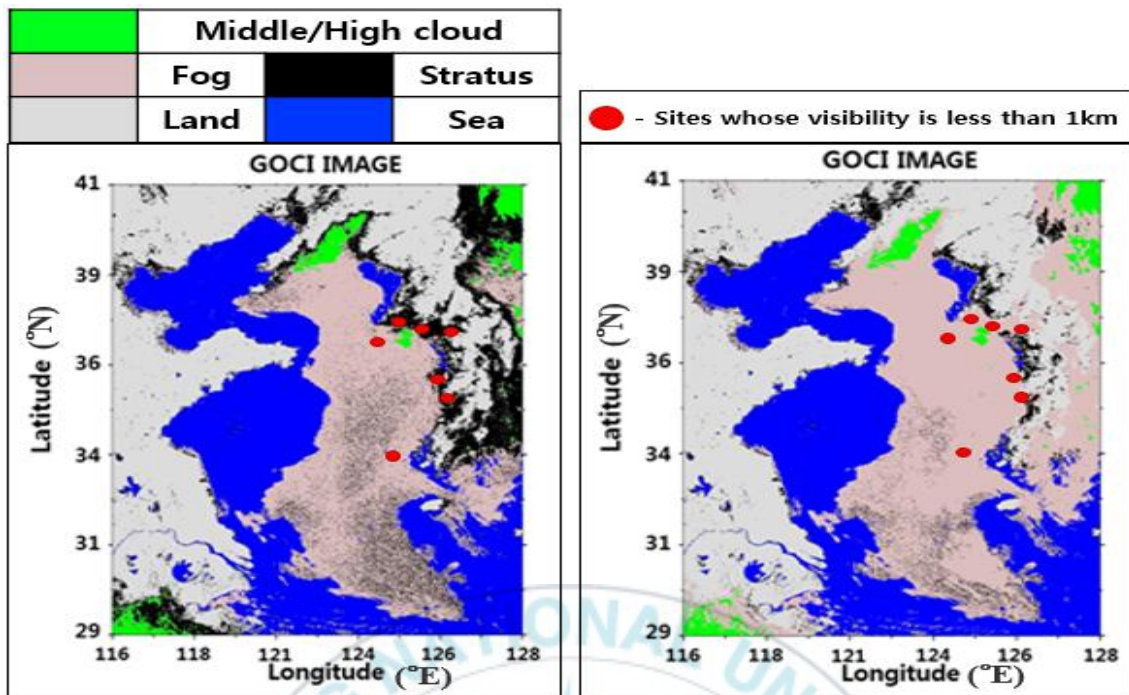


Fig. 18. GOCI fog image without threshold (left) and with threshold (right) in the Case 1.

Table 6. Quantitative validation on the threshold in the Case 1

Index	Before (west coastal)	After (west coastal)
POD	0.25	0.75
FAR	0.75	0.67
KSS	-0.5	0.08
TS	0.14	0.3
Number of site	35	35

For the second case, fog was not detected in the MI fog image. Hence, data from the visibility meter and visibility distribution was used to calculate the verification indices and compare the fog domains. The visibility distributions show that fog was observed in the northern Gyeonggi area near latitudes  $38^{\circ}\text{N}\sim 39^{\circ}\text{N}$  and longitudes  $126.5^{\circ}\text{E}\sim 128^{\circ}\text{E}$  and in the central area of the western sea near latitudes  $37^{\circ}\text{N}\sim 38^{\circ}\text{N}$  and longitudes  $126.5^{\circ}\text{E}\sim 127^{\circ}\text{E}$  (Fig. 19).

In the results, before the threshold was applied, fog was not detected in 8 sites where fog was observed (Table 7) (Fig. 20, left). On the other hand, after the threshold was applied, fog was detected at these sites, and the detected fog domain was similar to that of the visibility distribution (Fig. 20, right).

Upon calculating the verification indices, the POD was 0.333 and KSS was -0.417 before using the threshold, which are low results that imply that detection rate and detection level are low. After implementing a threshold, POD was 1 and KSS was 0.333, which is a drastic increase, and other indices had also improved (Table 8). Such results prove the usefulness of the GOCI that detected sea fog that was undetected from the MI.

Table 7. Visibility meter data of ASOS and AMOS  
in the Case 2

Site	Date	Visibility
Incheon airport	2015-02-11 09:00 KST	600 m
Dongducheon	2015-02-11 09:00 KST	80 m
Paju	2015-02-11 09:00 KST	50 m
Gimhwa	2015-02-11 09:00 KST	110 m
Ganghwa	2015-02-11 09:00 KST	50 m
Pocheon	2015-02-11 09:00 KST	920 m
Cheongsan	2015-02-11 09:00 KST	40 m
Yangju	2015-02-11 09:00 KST	10 m

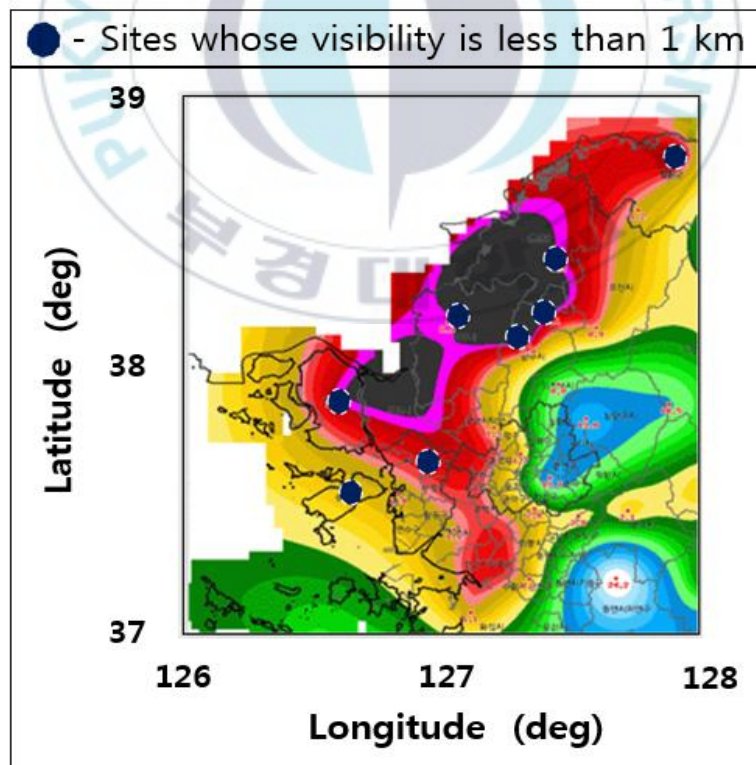


Fig. 19. Visibility map for the Case 2.

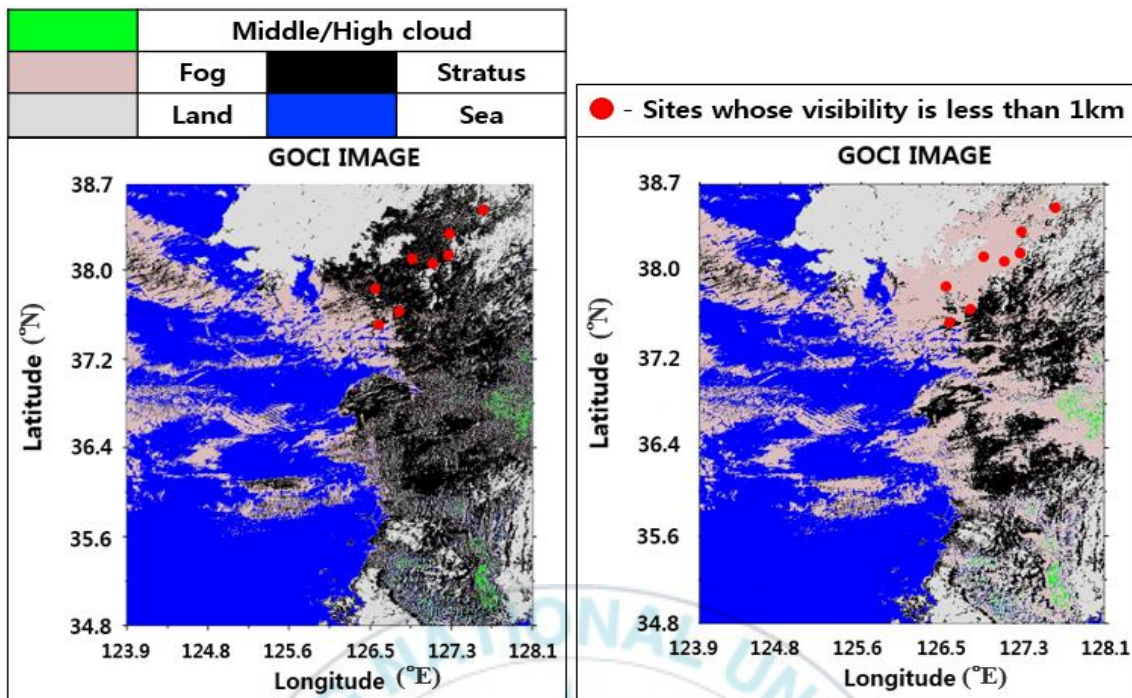


Fig. 20. GOCI fog image without threshold (left) and with threshold (right) in the Case 2.

Table 8. Quantitative validation on the threshold in the Case 2

Index	Before (west coast)	After (west coast)
POD	0.33	1
FAR	0.75	0.67
KSS	-0.42	0.33
TS	0.17	0.33
Number of site	39	39

In the third case, the visibility meter data shows that a low visibility of 9 m was observed at Baengnyeongdo island (Table 9), and a tail-shaped sea fog domain was detected on the seas above Baengnyeongdo island in the MI fog image (Fig. 21). Before the threshold was applied, the clouds over the seas above Baengnyeongdo island in the GOCI's sea fog detection results were categorized as sea fog like in the MI, but the clouds at Baengnyeongdo island were categorized as lower clouds (Fig. 22, left). On the other hand, after applying the threshold, thicker sea fog was differentiated than before in the seas above Baengnyeongdo island, and the clouds in Baengnyeongdo island were categorized as sea fog, which is consistent with the observed visibility (Fig. 22, right).

**Table 9. Visibility meter data in Yeongjongdo and Baengnyeongdo in the Case 3**

Site	Time	Visibility
Yeongjongdo island	2017-04-04 09:00 KST	6000 m
Baengnyeongdo island	2017-04-04 09:00 KST	9 m



## 2. False positive of sea fog

Because the clouds mentioned in Chapter 3 reflect the characteristics of the coordinates where they are located, Band 6 Rrc is greater than Band 7 Rrc for clouds at sea. This is the cause of sea fog overdetection in which the majority of clouds at sea are categorized as sea fog.

In order to resolve this issue, the spectral profile function of GDPS was used to analyze the Rrc of ocean pixels from Band 1 to Band 8. During spectrum profiling of ocean pixel, the Rrc value increased up to Band 4, then decreased until Band 8, creating a mountain shape (Fig. 23). These results are identical to the Index I calculation formula (Formula (1)) that differentiates the land and ocean; hence, Band 4 Rrc is always greater than Band 8 Rrc at the sea.

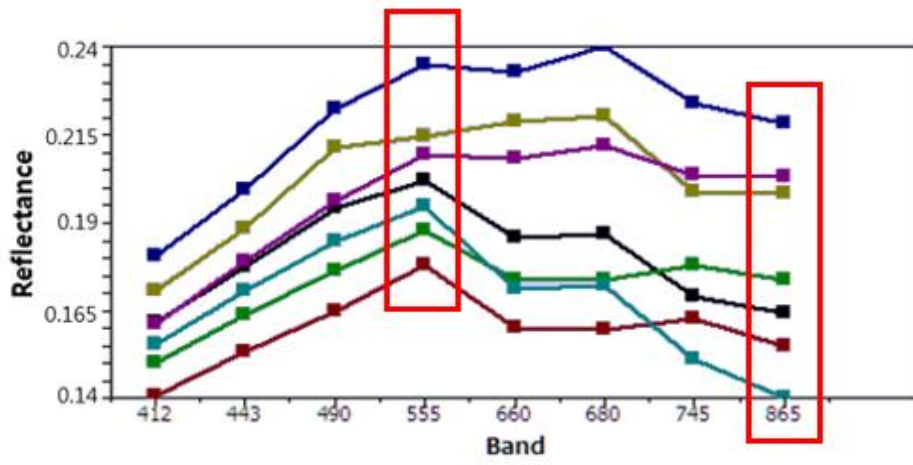
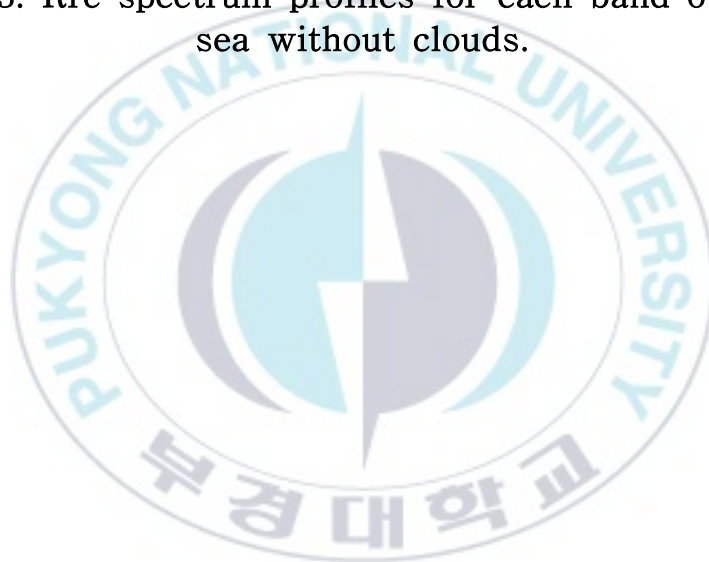


Fig. 23. Rrc spectrum profiles for each band over the sea without clouds.



To see if there are clouds with the above ocean characteristics from clouds at sea, pixels with a Band 4 Rrc that is greater than Band 8 Rrc were extracted around the central area of the western sea, which led to a river downstream area and the western coast (Fig. 24). In the index III, the cloud pixels in this domain are categorized as sea fog (Fig. 25), and this is a demonstration of the sea fog overdetection issue. Upon verifying whether or not sea fog actually occurred in this domain through the visibility distribution and MI fog image, it was clear that there was an overdetection of sea fog (Fig. 26, 27).



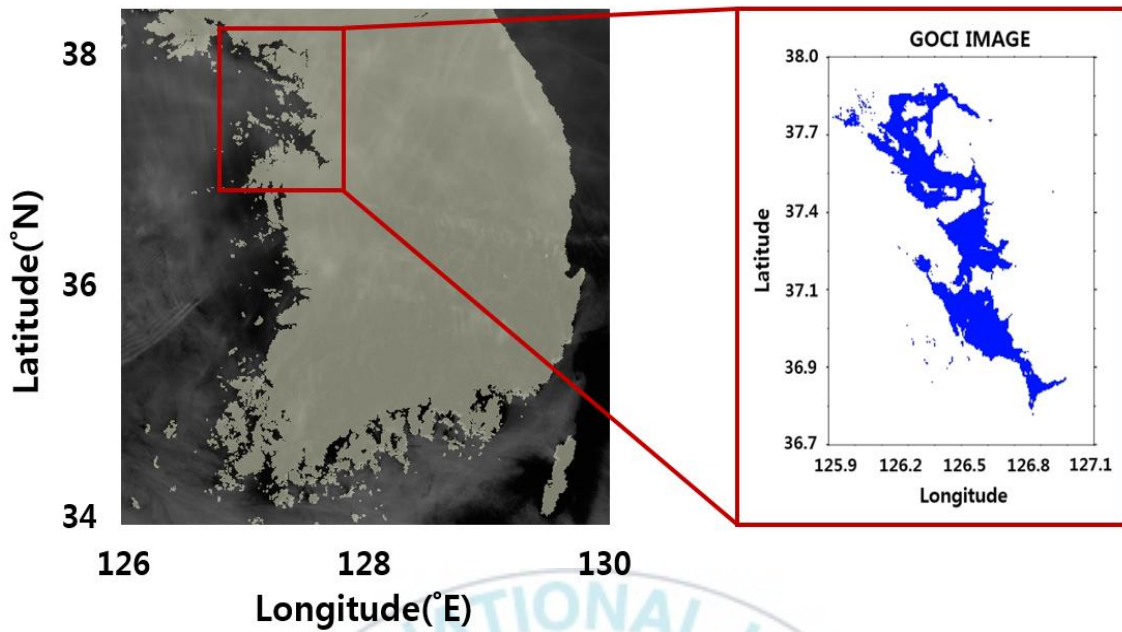


Fig. 24. Area for greater Band 4 Rrc than the Band 8 Rrc.

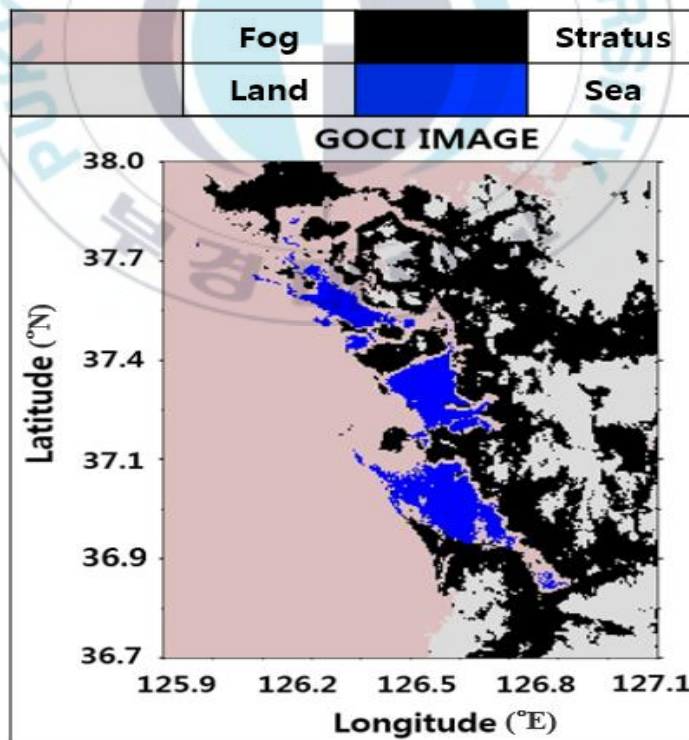


Fig. 25. GOCI fog image by index III at 09 LST on May 23 2014.

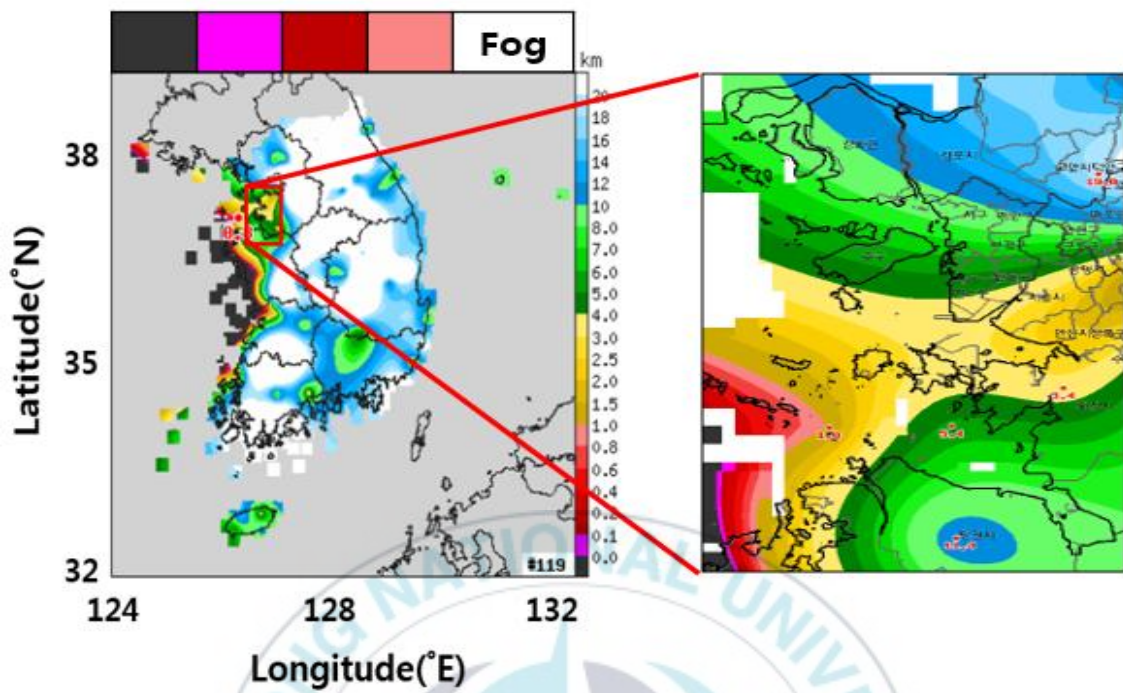


Fig. 26. Visibility map at 09 LST on May 23 2014.

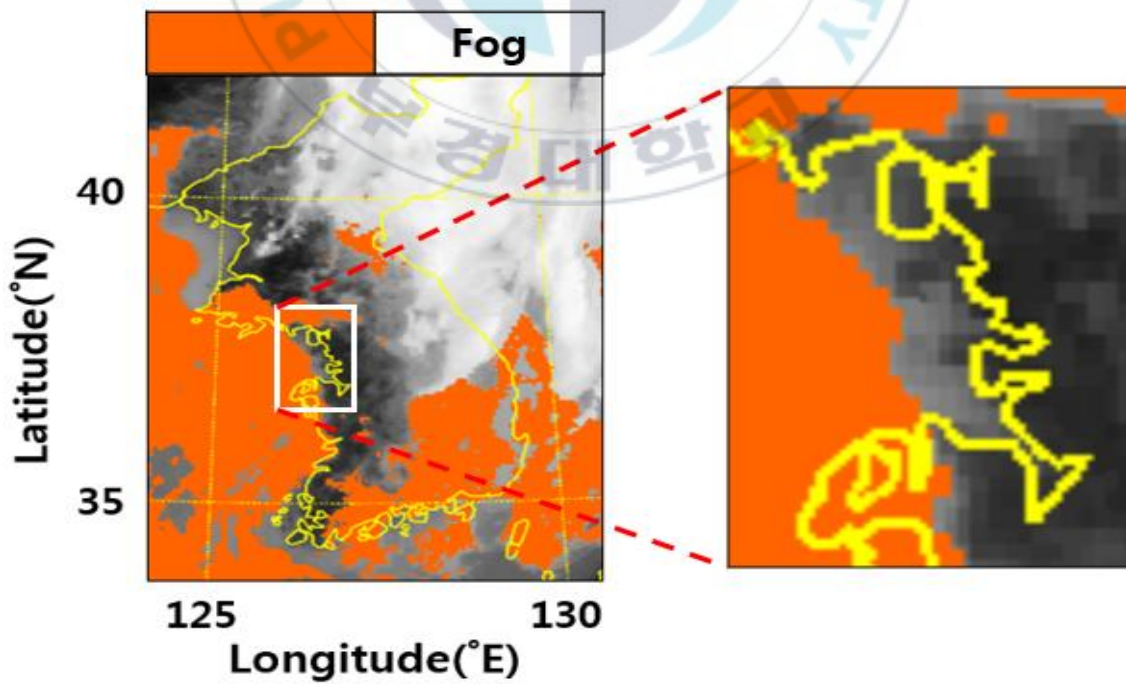


Fig. 27. MI fog image at 09 LST on May 23 2014.

In general, clouds have continuity, and this continuity can be utilized; if there is fog around the pixel when the fog detection rate is calculated, the fog detection rate increases for that pixel (Suh et al., 2017). Based on this point, the similarities between clouds that were incorrectly categorized as sea fog and the surrounding clouds were analyzed.

To analyze the overall similarity of reflectance, research was conducted in the following order. First, the reflectance was calculated for each overall band for cloud pixels in the central area of the western sea (Fig. 28, left box). Next, actual sea fog and lower clouds around the clouds that were incorrectly classified as sea fog were categorized (Fig. 28, right box). Finally, the reflectance of pixels that were sorted into three categorized were averaged to calculate the Mean Band Rrc (MBR). Before obtaining the MBR, pixels above a certain value were eliminated to remove discontinuity in the cloud domain. A linear trend line was used to remove these values. The linear trend line refers to one straight line that represents multiple data units. The final MBR value shows the average of this trend line, and this study used the middle value as the average value. Figure 29 shows the MBR calculation order for this study.

1	2	3	4	A	B	C	C
5	6	7	8	A	B	C	C
9	10	11	12	A	B	B	C
13	14	15	16	A	A	B	C

Fig. 28. Cluster sampling of cloud pixels.

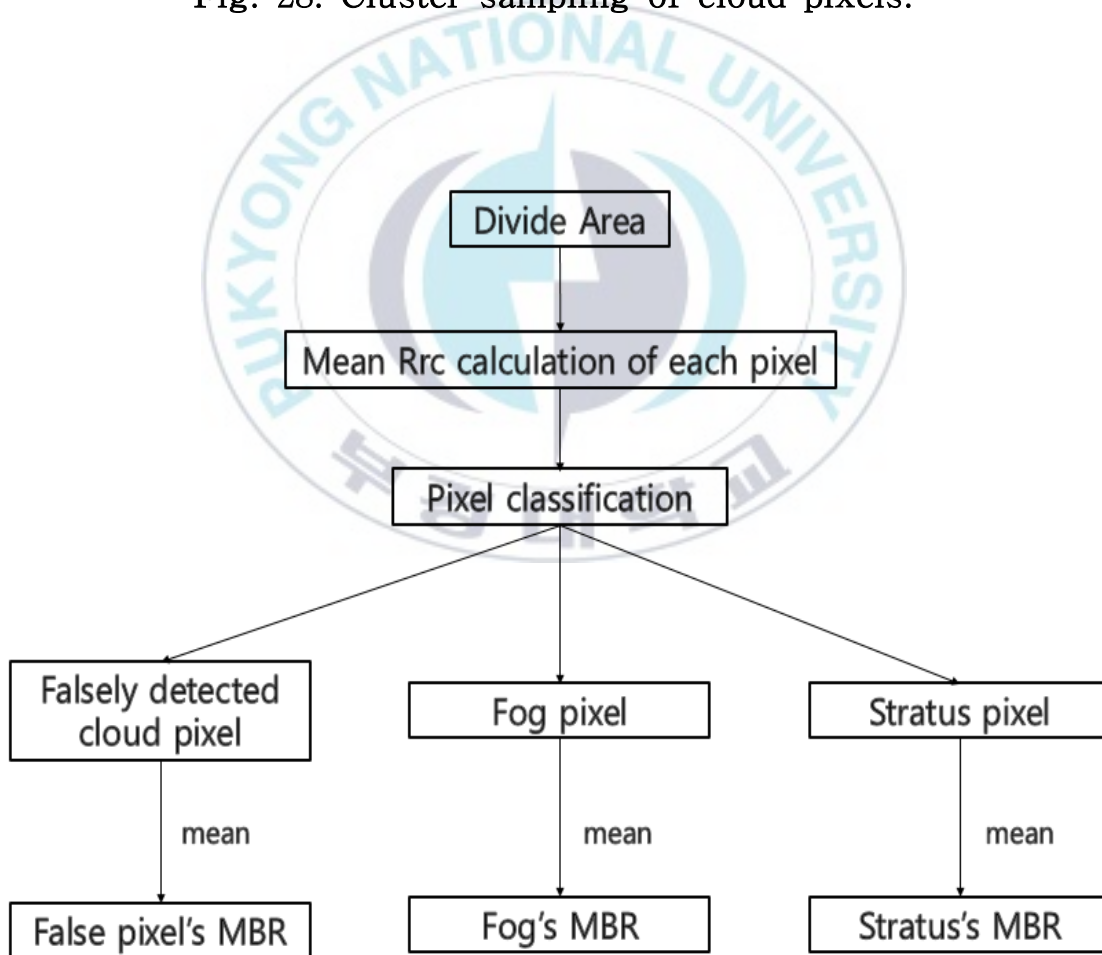


Fig. 29. MBR output flowchart.

Figure 30 shows the MBR value that was calculated as shown above. The cloud pixels that were incorrectly classified as sea fog (A) in Fig. 25 had an MBR of 0.2, the MBR of sea fog pixels (B) was 0.45, and the MBR of lower cloud (stratus) pixels (C) was 0.2. This shows that the MBR of the misdetected clouds and lower clouds is the same and that they have similar reflectance characteristics.



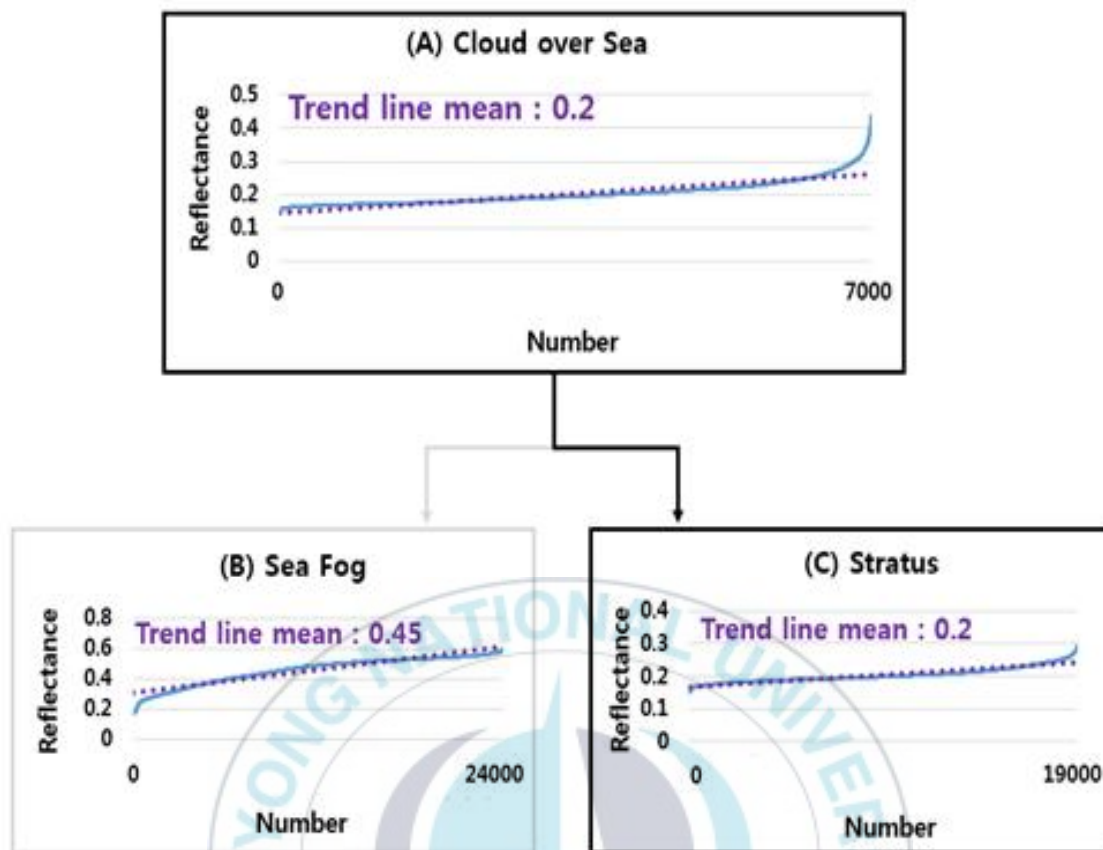


Fig. 30. Comparison of the MBR in (a) cloud over sea, (b) sea fog, and (c) lower cloud (stratus).

To find out if the MBR method correctly reflects the continuity of surrounding clouds, the correlation of individual cloud pixels was analyzed. First, the reflectance distribution of clouds that were sorted into three categories was analyzed through a box and whisker plot (Fig. 31). A box and whisker plot is a data distribution graph that shows where values are gathered and scattered, and calculates and shows quartiles. The box is divided into Quartile 1, Quartile 2, and Quartile 3 from the bottom, and each quartile refers to the 75th, 50th, and 25th percentile of data, respectively. The whiskers along the top and bottom of the box show the Inter Quartile Range (IQR) shown through Formula (8). The lower whiskers are calculated through Formula (9) and the upper whiskers are calculated through Formula (10).

$$\text{IQR} = \text{Quartile 3} - \text{Quartile 1} \quad (8)$$

$$\text{Lower whisker} = \text{Quartile 1} - 1.5 \times \text{IQR} \quad (9)$$

$$\text{Upper whisker} = \text{Quartile 3} + 1.5 \times \text{IQR} \quad (10)$$

Figure 31 shows how the average reflectance of false fog and stratus and the pixel distribution of Quartile 1 and 3 are similar as with the MBR. To draw the scatter plot for the three groups with different pixel quantities, stratified sampling was performed based on the group with the least amount of data, excluding values above a certain box and whisker range. Stratified sampling is a method that categorizes the target into several subgroups and extracts random samples from the small groups. It is used to prevent the extraction of population characteristics and other samples.



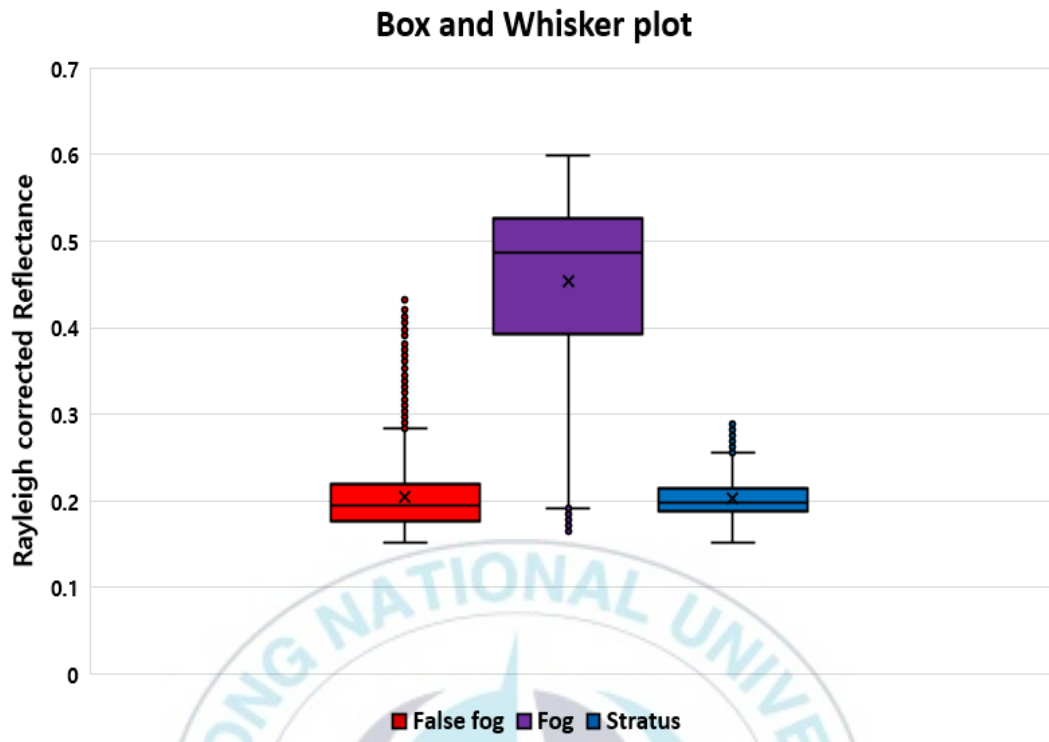
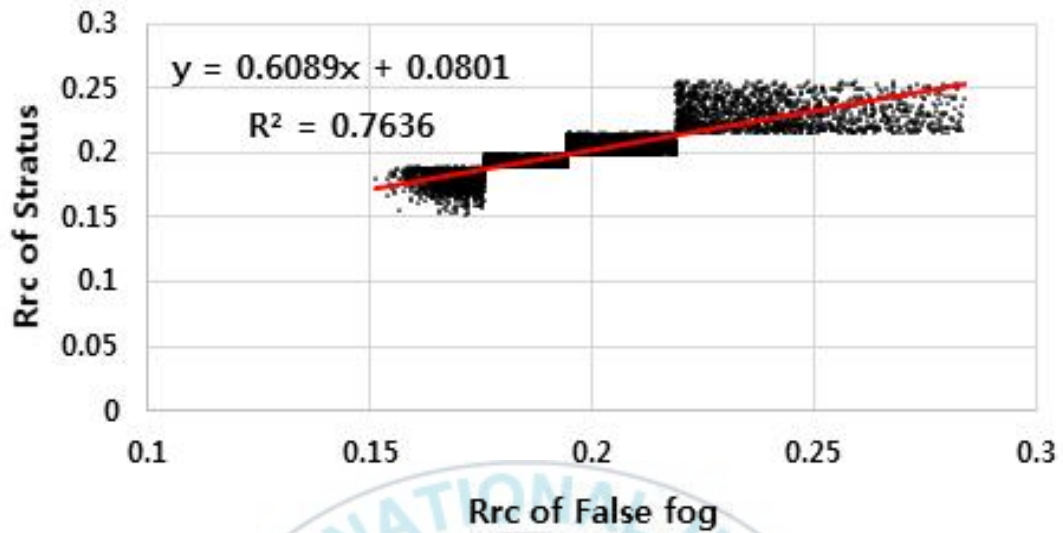


Fig. 31. Box-and-whisker plot of three groups (false fog, fog, stratus).

This study used 4 subgroups (Lower whisker: Quartile 1, Quartile 1-2, Quartile 2-3, Upper whisker: Quartile 3). Stratified sampling was performed on data from each subgroup based on the group with the smallest amount of data from the three groups (false fog in this case).

After stratified sampling, the scatter plot of false fog and fog, and false fog and stratus showed that the correlation coefficient in Figure 32-upper was about 0.76 and the X and Y-axis reflectance matching was similar. The correlation coefficient in Figure 32-lower was about 0.65 and there were differences in the X and Y-axis reflectance matching, which shows that correlation is stronger for stratus than sea fog. This is the same result as the MBR that was calculated above, which proves that the MBR value using cloud continuity correctly reflects the reflectance of clouds and is useful as a delimiter. Figure 33 shows the ascension of the stratified sampled data through a scatter plot; the correlation coefficient with stratus is about 0.98 and about 0.76 with sea fog. Therefore, correlation is stronger with stratus than with sea fog, as shown in Fig. 32.

### Scatter plot of False fog and Stratus



### Scatter plot of False fog and Fog

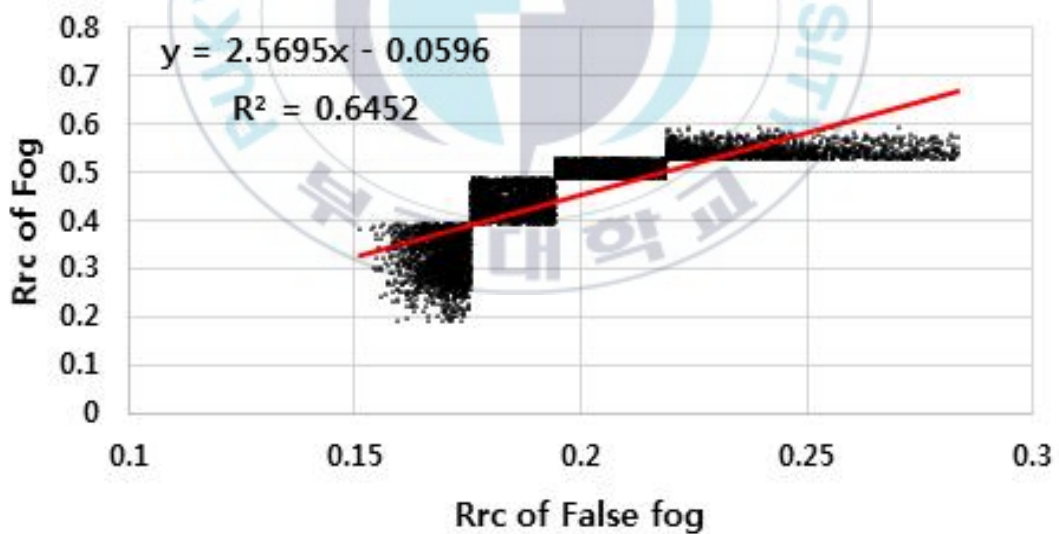
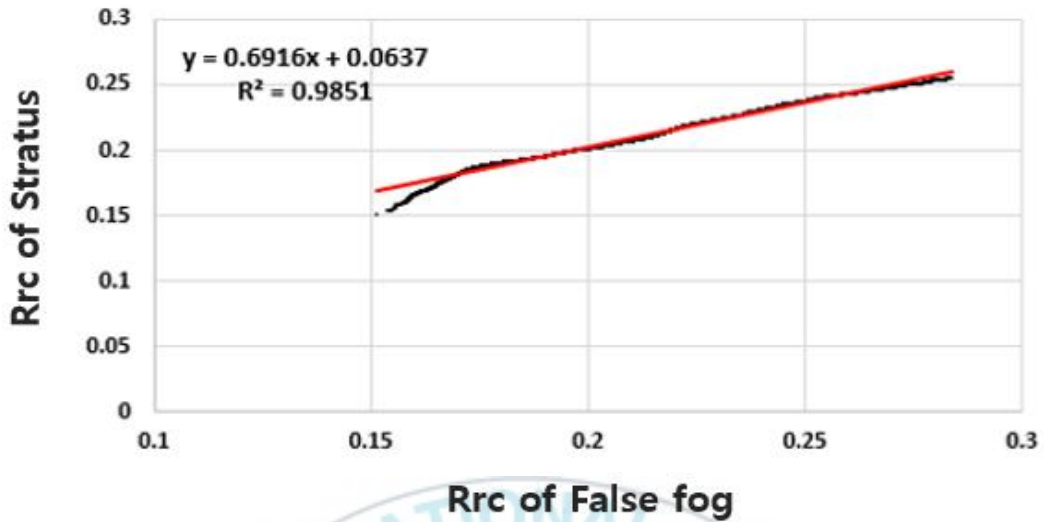


Fig. 32. Scatter plot of false fog and stratus (upper) and of false fog and fog (lower). The red line shows linear trend.

### Ascending scatter plot



### Ascending scatter plot

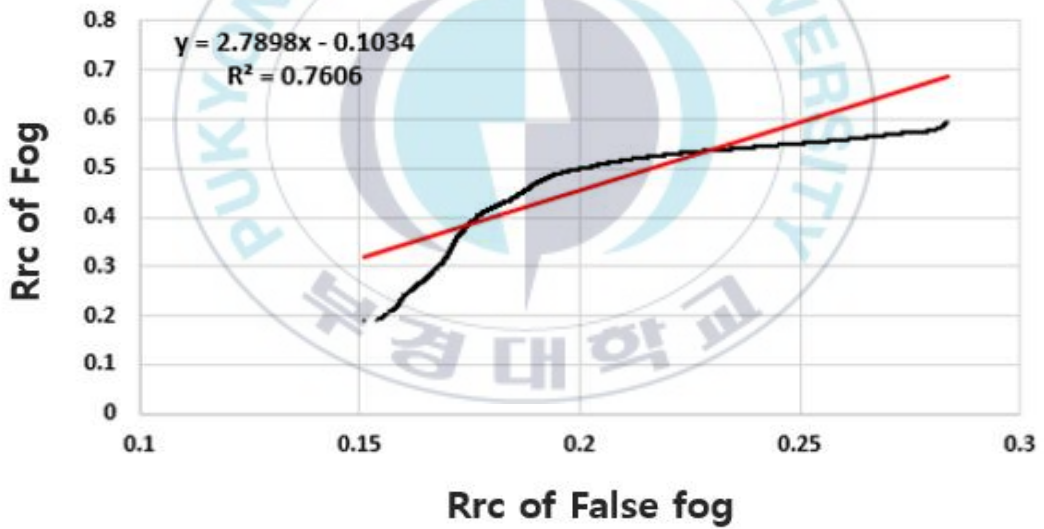
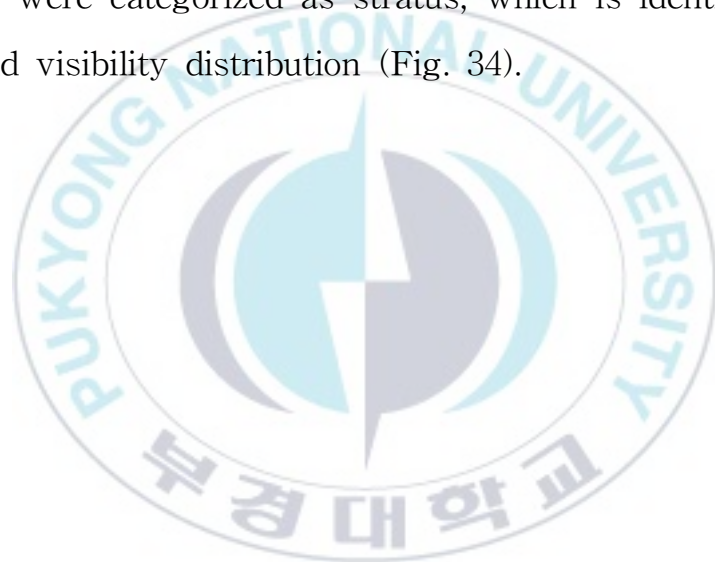


Fig. 33. Ascending scatter plot of false fog and stratus (upper) and of False fog and fog (lower). The red line shows linear trend.

The sea fog overdetection issue was improved by adding an algorithm that compares the MBR value of cloud pixels based on the above results and selects identical values.

In the Case 1, before MBR was applied, the clouds in the downstream area of northern Imjin river, around Yeongjongdo island, and the downstream area of southern Pyeongtaek lake were categorized as sea fog, unlike in the MI fog image and visibility distribution (Fig. 25). Upon applying the MBR method, the clouds in these regions were categorized as stratus, which is identical to the MI fog image and visibility distribution (Fig. 34).



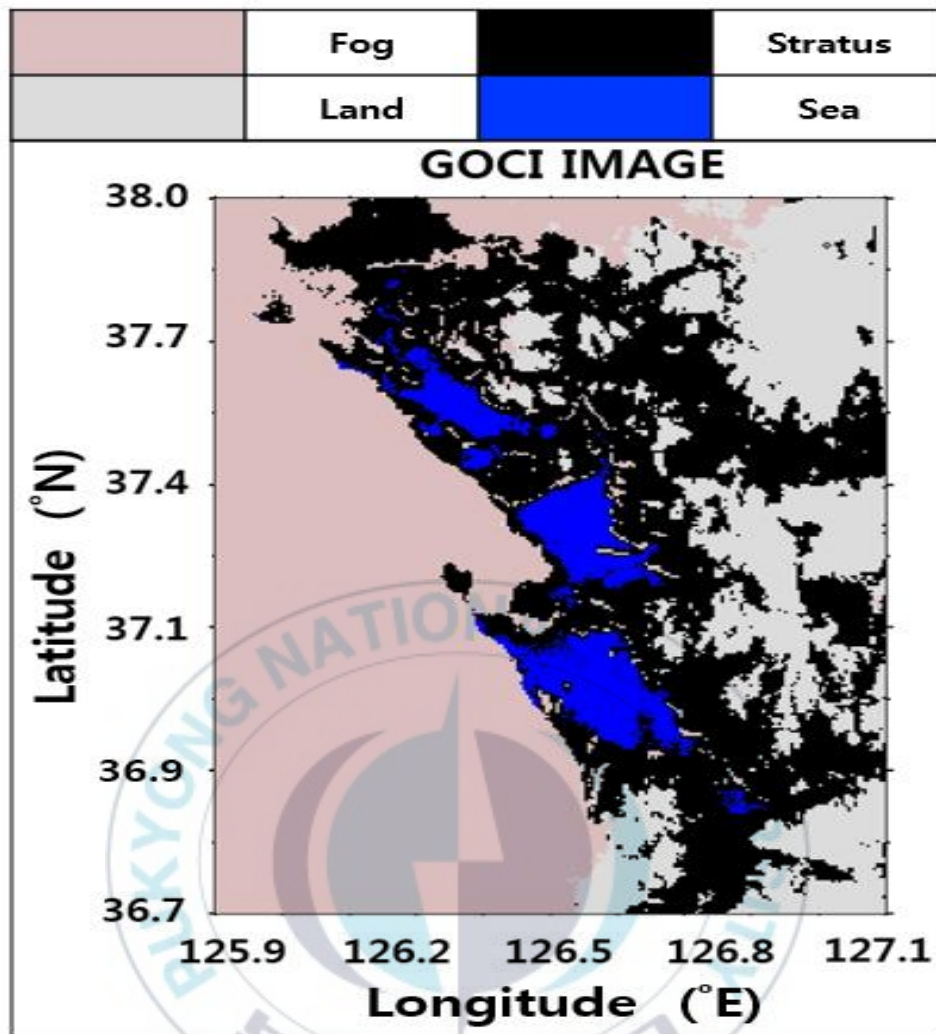
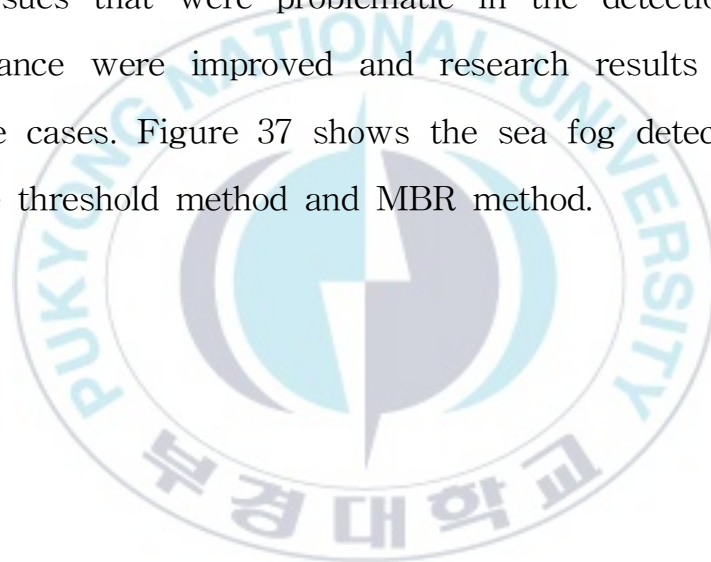


Fig. 34. GOCI fog image after MBR method applied in the Case 1.

In Case 3, before MBR was applied, sea fog was detected in red in the Imjin river basin of the western sea in the sea fog detection results (Fig. 35, upper). This contradicts the MI fog image, hence visibility under 1 km did not appear in these regions in the visibility distribution (Fig. 36). After MBR was applied, the clouds at the Imjin river basin that were detected as sea fog were now detected as stratus (Fig. 35, lower). Since this is consistent with the MI and visibility distribution, this implies that the MBR method is effective.

Two issues that were problematic in the detection of sea fog using reflectance were improved and research results were verified through three cases. Figure 37 shows the sea fog detection algorithm that adds the threshold method and MBR method.



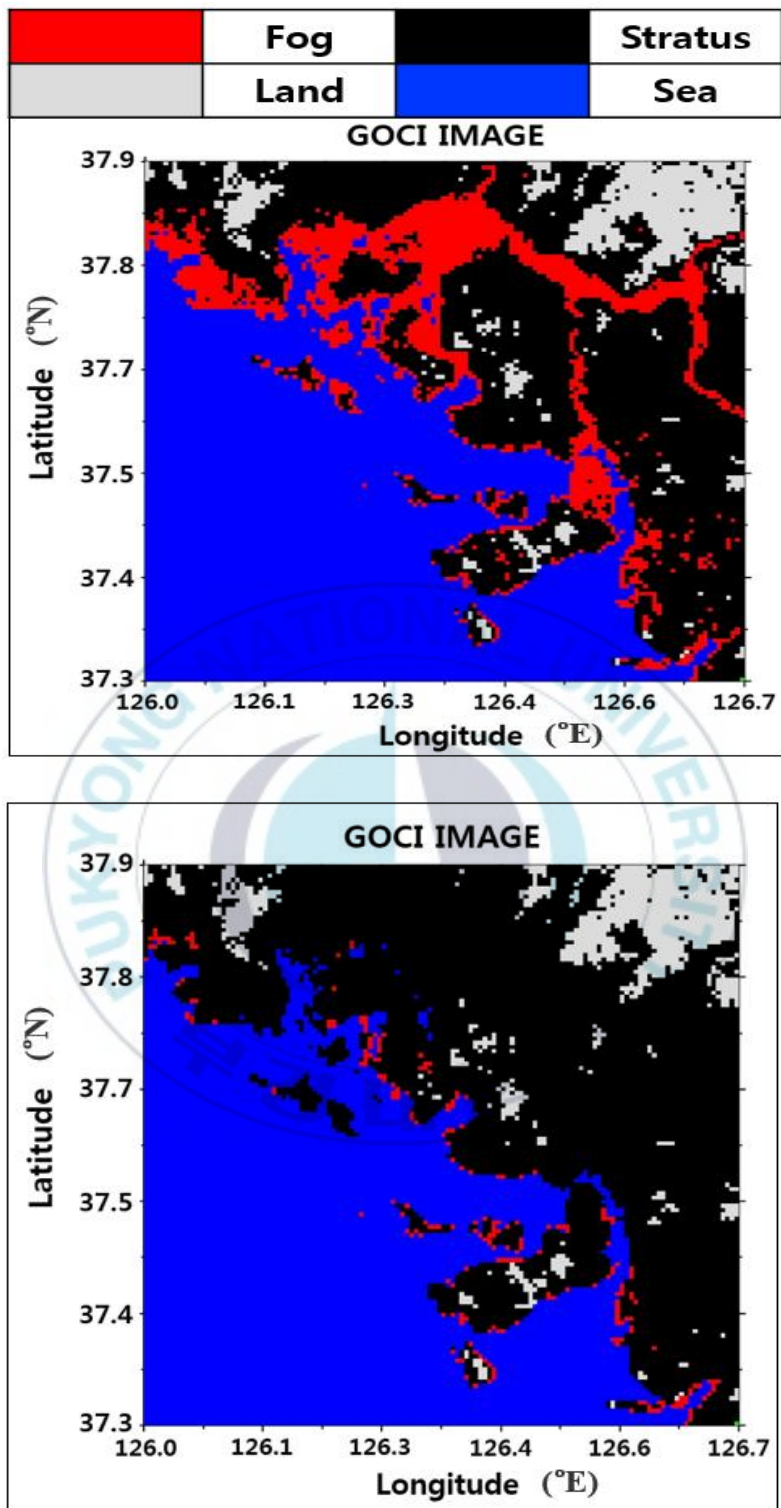


Fig. 35. GOCI fog image before (upper) and after (lower) MBR method application in the Case 3.

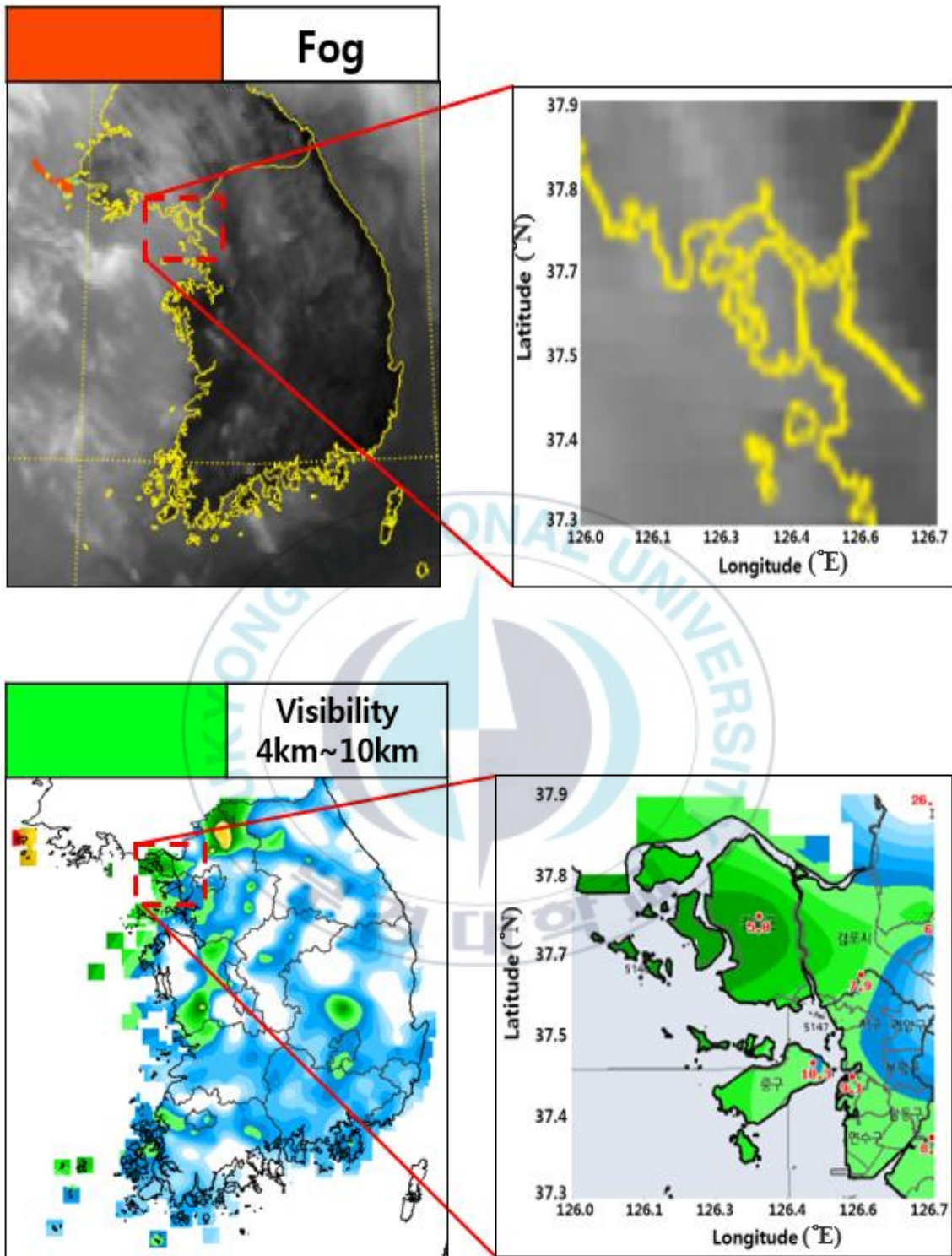


Fig. 36. MI fog image (upper) and Visibility map (lower) in the Case 3.

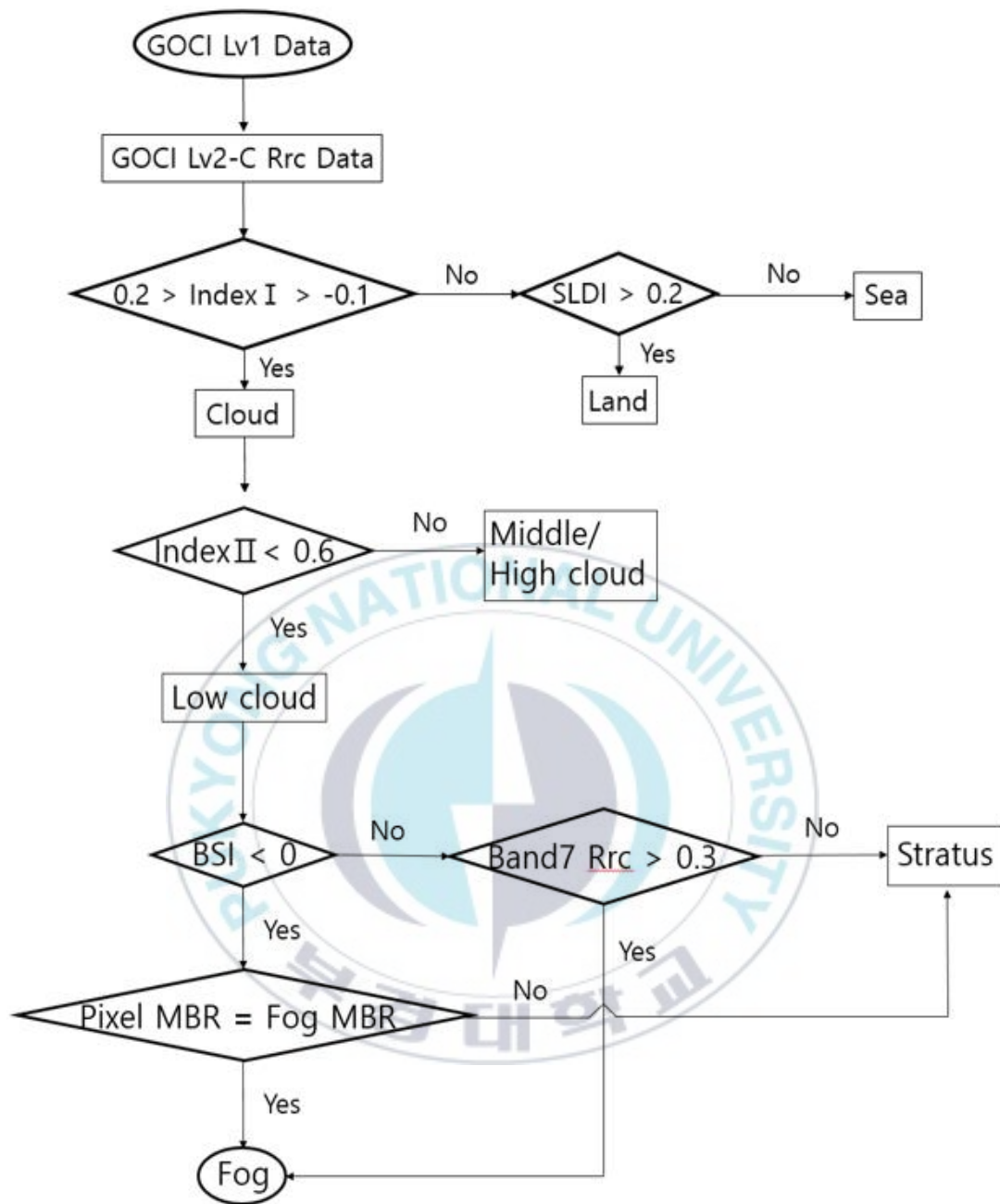


Fig. 37. GOCI sea fog detection algorithm applying Band 7 threshold and MBR.

## IV. Conclusions

Satellites remotely detect regions that are difficult to observe, such as the ocean, and can also be used for sea fog detection. GOCI can detect sea fog using the Rayleigh Corrected Reflectance.

This study improved the false negative fog flowing onto land areas by applying a threshold in the Band 7 Rrc. The false positive of sea fog was improved by comparing the MBR of cloud pixels with a large Band 4 and Band 8 Rrc difference. The threshold and MBR methods were applied to three cases.

In the first case, before the improvement method was used in the western sea region, the clouds that formed along the downstream of the entire western sea were overdetected as sea fog, and the sea fog that flowed into the western sea were undetected. This is contradicted by the MI fog image and visibility distribution data. After applying the improvement method, the results became more similar to the MI and visibility data. The POD was 0.25 before improvement and 1 after the improvement, which shows that the detection rate improved. The FAR was 0.75 before and 0.66 after improvement, showing that misdetection rate decreased. Further the KSS improved from -0.5 to 0.08 and the TS improved from 0.14 to 0.3, implying that the detection level and detection accuracy also increased.

In the second case, the fog in the northern and central regions of Gyeonggi of the western sea near latitudes  $37\sim 38.5^{\circ}\text{N}$  and longitudes  $126.5\sim 128^{\circ}\text{E}$ , which were not detected before applying the improvement method, were successfully detected, which are consistent with the visibility distribution. The POD improved from 0.33 to 1, the FAR improved from 0.75 to 0.66, the KSS improved from -0.41 to 0.33, and the TS improved from 0.16 to 0.33. In the third case, fog was detected at Baengnyeongdo island by visibility meter, but this fog was categorized as stratus. After applying the improvement method, the fog at Baengnyeongdo island was correctly differentiated and the sea fog domain was consistent with the MI image.

This study improved sea fog detection algorithm. However, because the research area was limited to the western sea region, there will be limitations in its ability to detect land fog, as the algorithm focuses on sea fog detection. Additional research is required in order to analyze fog that changes according to geology, season, and type. A number of accidents resulting from fog occurs during the daytime, such as the recent large-scale cancellations at Incheon Airport, the stranded passenger planes at Heuksando island, and the damage resulting from these accidents is only increasing. Therefore, GOCI with a higher spatial resolution for sea fog detection will greatly contribute to reducing accidents caused by sea fog at coastal areas and in the ocean.

## References

- Bendix, J., Thies, B., Cermak, J., Naul, T., 2005: Ground fog detection from space based on MODIS daytime data–A feasibility study. *Weather and Forecasting*, **20(6)**, 989–1005.
- Byun, H. R., Lee, D., Lee, H., 1997: Analysis on the Characteristics and Predictability of the Marine Fog over and near the East Sea. *Korean Meteorological Society*, **33(1)**, 41–62.
- Cho, H. J., 2003: Analysis of Hazardous Fog and Index Development in Korea. *Journal of the Korean Geographical Society*, **38(4)**, 478–489.
- Darko, K., 2017: Modeling and Forecasting Marine Fog. *Marine Fog: Challenges and Advancements in Observations, Modeling, and Forecasting*, 425–475.
- Ellord, G., 1995: Advances in the detection and analysis of fog at night using GOES multispectral infrared imagery. *Weather and Forecasting*, **10(3)**, 606–619.
- Eyre, J., Brownscombe, J., Allam, R., 1984: Detection of fog at night using Advanced Very High Resolution Radiometer (AVHRR) imagery. *Meteorological Magazine*, **113(1346)**, 266–271.
- Gultepe, I., Tardif, R., Michaelides, S., Cermak, J., Bott, A., Bendix, J., Jacobs, W., 2007: Fog research: A review of past achievements

- and future perspectives. *Pure and Applied Geophysics*, **164(6-7)**, 1121-1159.
- Heo, K. Y., Ha, K. J., 2004: Classification of Synoptic Pattern Associated with Coastal Fog around the Korean Peninsula. *Korean Journal of Atmospheric Sciences*, **40(5)**, 541-556.
- Heo, K. Y., Min, S. Y., Ha, K. J., Kim, J. H., 2008: Discrimination between Sea Fog and Low Stratus Using Texture Structure of MODIS Satellite Images. *Korean Journal of Remote Sensing*, **24(6)**, 571-581.
- Jeon, J. Y., 2016: Preliminary Study on Spring Season Daytime Sea Fog Detection Method Using MODIS in the Yellow Sea. *Department of Convergence Study on the Ocean Science and Technology School of Ocean Science and Technology Korea Maritime and Ocean University*.
- Kim, B. G., Jang, I. S., Lee, G., 2011: Real-time Road-Visibility Measurement Using CCTV Camera. *Journal of Korean Society of Transportation*, **29(4)**, 125-138.
- Kim, K. E., Min, K. D., Yoon, I. H., Park, S. G., 1995: Frequency Analysis of Fog Occurrence at Mt. Bohyun Astronomical Observatory. *Asia-Pacific Journal of Atmospheric Sciences*, **31(1)**, 35-44.
- Kim, M. O., 1998: (The) Characteristics of sea fog distribution around the Korean Peninsula. *Department of Oceanography Chonnam national university graduate school*.
- Kim, Y. A., Suh, J. Y., Yun, Y. H., Kim, J. H., 2003: A Fog Case

- Study Using Visibility Calculation Algorithm and Fog Prediction Model. *Atmosphere. Korean Meteorological Society*, **13(1)**, 432-435.
- Korea Meteorological Administration, 2015: Technology Form for Training Purposes to Forecaster(Intermediate level) Satellite Meteorology, 170-184.
- Korea Meteorological Administration, 2015: Favorite Forecast Techniques(No. 27).
- Korea Meteorological Administration, 2016: Annual Report 2016.
- Lee, H. K., Suh, M. S., 2018: A Comparative Study on the Visibility Characteristics of Naked-Eye Observation and Visibility Meters of Fog over South Korea. *Atmosphere. Korean Meteorological Society*, **28(1)**, 69-83.
- Li, Z., 2001: Studies of fog in China over the past 40 years. *Acta Meteorol*, **59**, 616-624.
- Mun, S. H., 2013: A Study on the Change of Fog Frequency and Duration hours in South Korea. *Department of Geography Graduate School of Konkuk University*.
- National Meteorological Satellite Center, 2013: Theoretical approaches to satellite-based meteorology. 21-134.
- Park, H. M., Kim, J. H., 2012: Detection of Sea Fog by Combining MTSAT Infrared and AMSR Microwave Measurements around the Korean peninsula. *Atmosphere. Korean Meteorological Society*, **22(2)**, 163-174.
- Suh, M. S., Lee, S. J., Kim, S. H., Han, J. H., Seo, E. K., 2017:

- Development of Land fog Detection Algorithm based on the optical and Textural Properties of Fog using COMS Data. *Korean Journal of Remote Sensing*, **33(4)**, 359–375.
- Sheng, P., Mao, J., Li, J., Sang, J., Pan, N., 2003: Atmospheric Physics. *Peking University*, 11.
- Shim, H. N., Lee, Y. H., 2017: Influence of Local Wind on Occurrence of Fog at Inland Areas. *Atmosphere. Korean Meteorological Society*, **27(2)**, 213–224.
- Won, D. J., Kim, S. Y., Kim, K. E., Min, K. D., 2000: Analysis of Meteorological and Oceanographic Characteristics on the Sea Fog over the Yellow Sea. *Atmosphere. Korean Meteorological Society*, **36(6)**, 631–642.
- Yang, H. Y., Oh, S. N., 2005: Investigation on Cloud Properties for Fog Modification at Daegwallyeong Mountains. *The Magazine of the Korean Society of Hazard Mitigation*, **5(2)**, 45–56.
- Yoon, H. J., 2018: Ocean Remote Sensing(Utilization of Big Data of 4<sup>th</sup> Industrial Revolution and Ocean Remote Sensing), 5–18.
- Yuan, Y., Qiu, Z., Sun, D., Wang, S., Yue, X., 2016: Daytime sea fog retrieval based on GOCI data: a case study over the Yellow Sea. *Optics Express*, **24(2)**, 787–801.